Combined Multibody Musculoskeletal Dynamic Modeling and Finite Element Modeling of the Human Tibia in Countermovement Jumps

by

Merwa Al-Rasheed

A thesis

presented to the University of Waterloo

in fulfillment of the

thesis requirement for the degree of

Master of Applied Science

in

Systems Design Engineering

Waterloo, Ontario, Canada, 2021

Author's Declaration

I hereby declare that I am the sole author of this thesis. This is a true copy of the thesis, including any required final revisions, as accepted by my examiners.

I understand that my thesis may be made electronically available to the public.

Abstract

Computational models have been used to examine and estimate various motions and loading conditions of the human body that are otherwise difficult to examine experimentally. To study human musculoskeletal dynamics, biomechanical multibody models can be utilized with inverse or forward dynamics. To study the stress and strain response of complicated geometries, such as bones, finite element models can be utilized under specific loads and boundary conditions. When examining an injury mechanism or studying a specific motion, tackling both areas of computational modeling can provide insightful information (e.g. reaction forces or stress distribution. This thesis presents the work of combining a musculoskeletal dynamic model and a finite element model to examine the dynamics of countermovement jumping and the resulting stress on the human tibia.

The objectives of this thesis were to study the impact dynamics and investigate the stresses and strains of the human tibia during countermovement jumping. This work utilized multibody dynamic modeling and finite element modeling to investigate the risk of injuries in a jumping-landing motion. Initially, experimental data of position and ground reaction forces were obtained from a subject during countermovement jumping. This data is utilized in an inverse kinematics analysis to obtain joint angles of the lower extremity. A multibody model was constructed with segment lengths and parameters that are specific to the subject. The human was represented as four rigid links in the sagittal plane connected with revolute joints. Inverse dynamics was applied on the model with inputs of angles and positions of countermovement jumping to provide joint torques. Following that, a static optimization was performed to obtain muscle forces, while tackling the problem of redundancy. A total of 9 muscles were defined in the model and included in the static optimization problem under the objective function of minimizing muscle stress. With obtaining muscle forces, joint contact forces were also computed. Finally, a finite element model of the tibia was used to examine the stresses and strain under calculated loads of countermovement jumping. With a countermovement jump, the flexion/extension torques about the hip, knee, and ankle were slightly higher during the jumping phase than the landing phase. However, the stresses and strains were higher in the medial shaft of the tibia during landing phase than during jumping. This suggests that an injury to the tibia (i.e. stress fracture) is possible at locations of lower cross-sectional area under repetitive impact loads and elevated stresses of countermovement jumps.

This framework provided a potential of examining motion dynamics and structural bone response of the human body under loadings specific to the motion studied. It can be utilized as a tool for training in sports, or as a tool in prevention of injury in specific motions. This work also provides the first documented investigation that compares a finite element analysis of jumping and landing.

Acknowledgment

For the past two years, I have worked on this project to obtain my master's degree. At first, I did not know what to expect and I was constantly worried about my potential. After six months, the pandemic hit, and working on this project got much harder. With all the difficulties I faced, I would like to acknowledge and thank those who helped in reaching a new milestone in my life.

Most importantly, I would like to thank and express my appreciation to Prof. John McPhee and Prof. Thomas Willett for all the help and support with this work. This work started off from a simple idea during a discussion and it grew to a project that I am very proud to have completed. They provided full guidance and support throughout this project. Prof. McPhee's words of affirmation and the constant feedback always managed to keep me motivated. Prof. Willett on the other hand always managed to keep me trying harder to achieve a better outcome. They are both very supportive, understanding, and thoughtful and I appreciate it very much. Thank you for being my advisors, I am very lucky to have been your student.

With the pandemic, several parts of my work were affected, and it became possible with the help of some extraordinary people. I would like to thank Prof. Stacy Acker and Natasha Ivanochko at the University of Waterloo for providing experimental data for this work. I would also like to thank Prof. Brent Edwards and Ifaz Haider for providing a tibia model for the finite element analysis. With their help, I was able to tackle the hardships and complete this work.

Throughout my degree, I had the privilege to work with amazing members of the Motion Research Group and the Composite Biomaterial Systems Lab. Every member inspired me to do better and helped me out whenever I stumbled on a problem. I am very thankful and happy to have worked with amazing colleagues. I would especially like to show my appreciation to Mahdokht Ezati, Valerie Norman, Daniel Dapaah, and Ali Asghar Mohammadi for all the help they provided.

I would also like to acknowledge the Natural Sciences and Engineering Research Council of Canada for funding my research.

Lastly, I would like to thank my family and friends for their emotional support and for believing in my potential for the past two years. I experienced many ups and downs while working on my thesis, but they always supported me in every way and I really appreciate it.

Table of Contents

List of Figures

List of Tables

Chapter 1

1 Introduction

Jumping is a common movement performed by humans. People tend to jump while playing several sports, exercising, dancing, or simply while running around. Jumps can be differentiated by many factors that include frequency, height of the jump, or the type of jump itself (vertical jumps, slackline jumps, skip jumps, etc.) [1]. Jumps require the body to exert some force to achieve a certain height, and similarly, landing after jumps imposes impact forces on the body. These impact forces resulting from jumping and landing can affect the condition of bones, ligaments, and tendons of the body [1]. This thesis covers a study of computationally combining a multibody musculoskeletal dynamic model of a human during a jumping-landing motion with a finite element analysis of the tibia. Specifically, countermovement jumping is the motion analyzed for this work. It involves a squatting motion, followed by a vertical jump to a maximum height.

1.1 Problem Description

Several sports are associated with lower-extremity injuries that vary in severity and can have a detrimental effect on athletes [2]. These injuries are usually associated with power movements, such as jumping, landing, running, twisting or other sudden motions [2]. Understanding injury mechanisms gained interest in the research community, mainly aiming to derive a pathway to reduce the risk of injuries [2]. However, each sport is unique and imposes a different risk of injuries to different parts of the lower extremity. Many common injuries during sports have been studied superficially, but few studies have gone in-depth to analyze various factors that can potentially cause these injuries [2-5].

Stress fractures in bones of the lower extremity account for about 20% of all sports-related injuries [3]. Each sport is generally correlated to stress fractures of specific bones, at specific locations [3]. For example, running is associated with a higher prevalence of stress fractures in the shaft of the tibia and fibula [3]. There are many factors that can lead to stress fractures in bone, and biomechanical analysis has been used previously to provide some insight [2]. In sports, the frequency, the type of motion, and the sudden changes to the motion could be some of the factors that lead to injuries in the lower extremity [4].

Jumping and landing are two common movements that take place in many sports, such as basketball and volleyball [2]. Impact forces are associated with such movements and thus higher risk of injuries is usually expected [5]. However, many variations of jumping and landing exist in sports [2]. Countermovement jumping (CMJ), also referred to as squat jumping from a standing position and hand placed still on waist, can impose high loads on the body at very high speeds [5]. CMJ is used to evaluate the capabilities of athletes, while reducing the effects of several variables such as arm swings and athlete's intent [6].

Musculoskeletal modeling has been used frequently for many biomechanical applications, primarily due to ethical and invasive barriers to directly measure joint contact forces, muscle forces, and muscle length changes [2]. It provides a dynamic analysis of motions that can cause musculoskeletal sports injuries, as it allows estimating muscle forces and joint loads [2]. It has been mainly used for activities of daily living, and less frequently for activities of faster execution or higher loading (requires higher complexity in modeling) [5]. Several studies have conducted multibody modeling during jumping or landing; however, they were mostly focusing on the dynamics of the motion and its correlation to some injuries (ACL injury) [7-11].

Finite element analysis has been used in biomechanical research to simulate the stress/strain distribution in bone [4]. The accuracy of these models has been often compromised due to inaccurate/ nonspecific input data to the model, along with extremely simplified geometry [4]. For example, a bone model can be loaded at simplified locations by a ratio of the bodyweight [12]. This can provide some insight into the motion; however, it cannot lead to realistic observations that can be used to prevent injuries. Thus, it is important to have realistic loadings that correlate to the motion studied and incorporate bone adequate bone properties (geometry, material strength and boundary conditions) to have greater confidence in the finite element analysis [4].

1.2 Research Goals and Contributions

This research had two main goals. The first goal of this work was to study the impact dynamics of a countermovement jump. The second goal of this work was to analyze the stresses and strains in the human tibia during a countermovement jump. Musculoskeletal modeling can provide important information about factors that affect the motion, which include joint torques, joint contact forces, and muscle forces. Finite element modeling can examine the response of a specific bone under the loads occurring during the motion studied. Overall, this work aims to combine two important simulation techniques, multibody dynamic modeling and finite element modeling, towards investigating the risk of injuries during a jumping-landing motion.

To tackle this research problem, the project was subdivided into 6 phases. Phase I of the work was the collection of experimental data of countermovement jumping, which included capturing data of position and ground reaction forces of a subject. Phase II of this work involved inverse kinematics, which utilized experimental data to obtain joint angles of the lower extremity of the body. Phase III of this work was the construction of a biomechanical model, which is a 2D skeletal sagittal model with 4 rigid bodies and three revolute joints. Phase IV of this work was an inverse dynamic analysis using the multibody model, with experimental joint angles, ground reaction forces, and position of the pelvis, to obtain joint moments and moment arms of several major muscles. Phase V of this work was a static optimization analysis to compute muscle forces acting on the tibia. Phase VI of this work was a finite element analysis of the tibia under loads obtained in phase IV and phase V, to examine stress, strain, and deformation of the bone during jumping and landing. A flowchart of this work is provided in Figure 1.

This work aims to contribute to the fields of multibody biomechanical modeling and finite element modeling of bone. The main contribution is providing a framework to obtain motion-specific and meaningful loads for the stress analysis of bone, rather than the current approach of using approximate loads that are relevant to bodyweight [12]. This framework can be used to give a greater insight into risk injuries in sport-related motions, specifically the jumping-landing motion. A reverse of this framework can also be used in the future to obtain optimal motions, while ensuring better stress distribution in bones and lower risk of injuries. Moreover, this work may be used as a potential tool for training athletes to enhance performance, while reducing the risk of injuries.

To the best of the author's knowledge, there have been no previous finite element analyses that examined both jumping and landing. This work introduces the ability to analyze the full motion and allows a realistic comparison between jumping and landing and its effects on the human tibia.

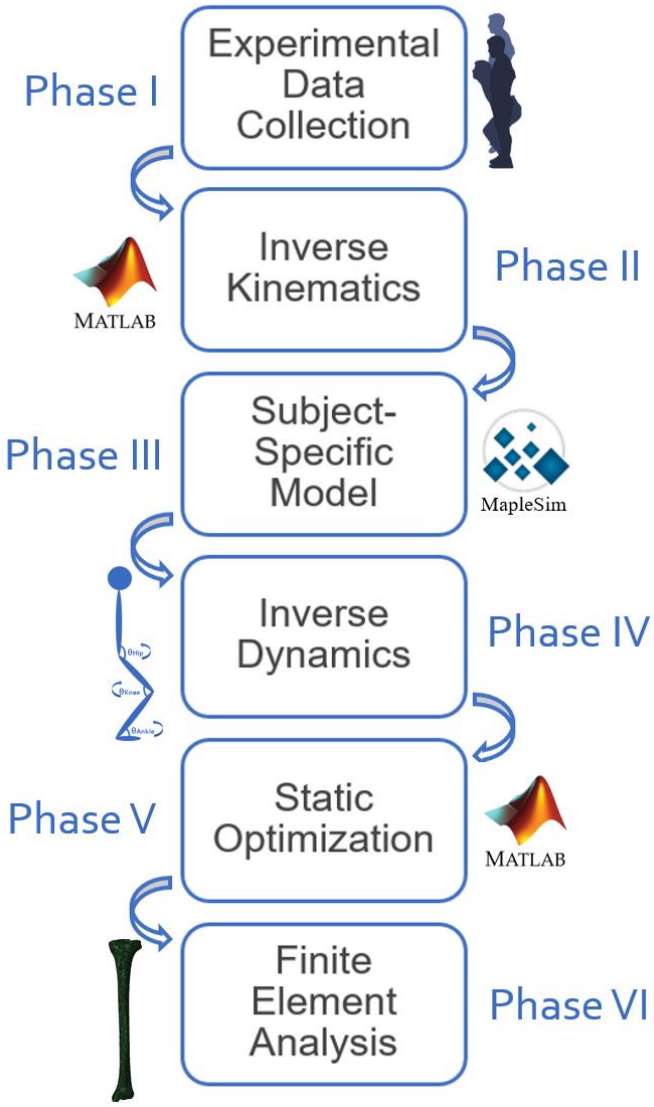

Figure 1: Flow chart of the method process utilized for this thesis

1.3 Thesis Structure

This thesis consists of seven main chapters. Chapter 1 is the introduction of this thesis, which consists of the objectives and contributions of the work presented in this thesis. Chapter 2 is a literature review, which includes information about previous research on countermovement jumps, dynamic modeling, stress fracture in bones, and the merge of multibody dynamic modeling with finite element modeling. Chapter 3 reports on the construction of a multibody biomechanical model, which includes collecting and analyzing experimental data, along with the design of the biomechanical model. Chapter 4 reports on the dynamic simulations, which are the result of an inverse dynamic analysis of the multibody model. Chapter 5 concerns the muscle forces, which includes the use of static optimization and the application of a numerical and an analytical approach to obtain muscle forces from joint torques. Chapter 6 reports on the finite element model of the tibia, which includes the various steps and results of a finite element analysis of the tibia during a countermovement jump. Chapter 7 is the conclusion of the thesis, including a limitations section and recommendations for future work that can be applied to this framework.

Chapter 2

2 Literature Review

This chapter is a review of existing research that has inspired the work of this thesis, along with background knowledge for different aspects of this project. The literature review is divided into 4 sections, which tackle theoretical explanation and previous research in various fields of this work. Section 1 describes countermovement jumping, the different phases of the jump, and the use of the jump to evaluate the performance of athletes. Section 2 describes the difference between inverse dynamics and forward dynamics in simulated models. Section 3 examines stress fractures and their prevalence in sports. Lastly, section 4 investigates previous literature that tackled the method of combining multibody dynamic modeling to finite element modeling.

2.1 Countermovement Jumps

Countermovement jump (CMJ) is a type of vertical jumping that is used to monitor athlete performance, as it is consistent and non-fatiguing [13-14]. Primarily, CMJ is a tool to assess the power of the lower extremity of athletes in many sports, such as basketball and volleyball [6]. It can assess the jumping height of athletes, along with providing insight about velocity, power, and forces attainable [13]. The study of the force-time curve of the CMJ motion has gained attention in the research of sports biomechanics [13]. Previous research investigated different factors that can influence the force-time curve of CMJ in athletes, such as effort exerted, depth of jumping, or neuromuscular training [13, 15-17].

CMJ is defined as a jump that initiates with a countermovement motion, as the body goes into a squatting position, to be followed by a jump to the maximum height possible [18-19]. In CMJ, the hand is usually placed still on the hips to eliminate possible momentum generated by arm swings that could affect jumping height and the motion itself [6]. Biomechanically investigating the different stages of the jump can provide a qualitative measure of assessing the effectiveness and effort of the individual, mostly through examining peak forces [6]. To increase the height of CMJ, it is recommended to increase the depth of squatting, have larger countermovement, and larger inclination of the trunk [19-20]. To measure the performance of CMJ, force plates are usually used to quantify vertical forces throughout the motion [18].

Overall, the motion can be broken down into 5 different stages. Figure 2 depicts a simplistic representation of these different stages. Stage 1 is the standing stage, which indicates the beginning of the motion by quite standing [21]. The vertical force that is usually measured during this stage corresponds to the weight of the individual [21]. Stage 2 is the unweighting stage, which corresponds to a downward squatting motion to lower the center of mass [18]. This takes place when the individual flexes the hip and knees with a downward acceleration, while it ends when the center of mass reach its lowest height prior to attempting the jump [21]. The vertical force that is usually measured during this stage is lower than the weight of the individual [21]. The unweighting stage is also referred to as the eccentric phase when examining muscles [22]. This is when the subject stores elastic energy in muscles and tendons to provide enough energy for the jump [6]. The subject does not hold the squatting position, but rather variable speeds can be attainable during the unweighting stage that can affect the performance [21]. Stage 3 is the propulsion stage, which corresponds to an upward motion from the lowest position of stage 2 and until take-off [6]. A peak vertical force is usually measured that is larger than the bodyweight of the individual, where a higher force could correspond to a larger jumping height [21]. The propulsion phase is also referred to as the concentric phase when examining muscles [22]. The elastic energy that is stored is utilized in this stage for muscles to exert enough force for the jump against the force of gravity [6]. Take-off point is an important term when describing the CMJ motion, which indicates that the jumper's feet are off the ground completely [21]. It is the point that separates stages 3 and 4, the propulsion stage and the jumping stage. Stage 4 is the jumping stage, which corresponds to an upward motion with feet being completely off the ground and the center of mass being higher than that of the standing stage [21]. Athletes are usually instructed to provide maximal effort during the jump phase to achieve a higher jump, while ensuring that the legs are extended [18]. Stage 5 is the landing stage, which indicates a balancing motion from the point that feet touch the ground and until a standing stance is achieved [21]. Two peak vertical forces are usually measured during this stage [21]. The first peak force is higher in magnitude than the second, which is an indication of an impactful force due to landing [21]. This peak force is usually the highest vertical force to be measured during a CMJ [21]. The second peak measured is due to attempts of balancing, which is usually due to slight squatting and propulsion [21]. This peak force is typically variable between different jumps and different individuals [21].

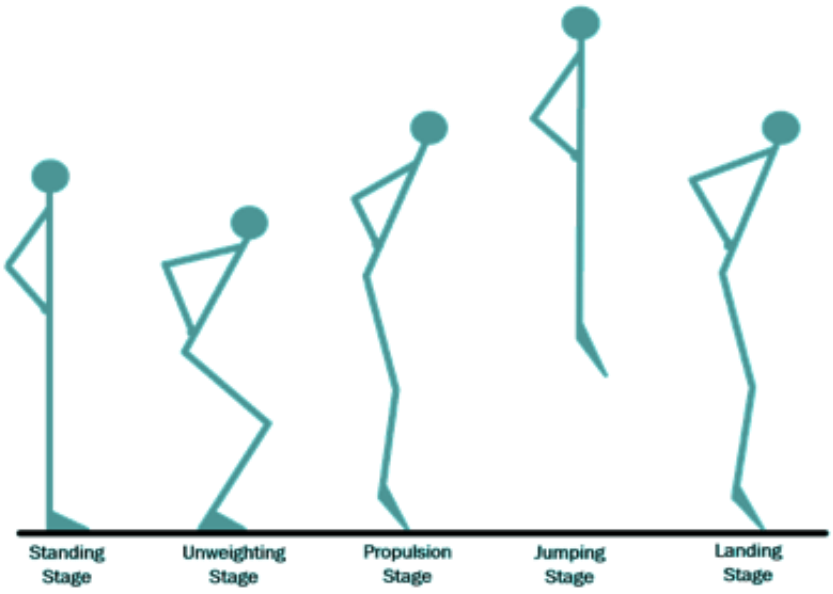

Figure 2: Simple illustration of the different stages of a countermovement jump

In previous CMJ research, the individual is instructed during the unweighting stage to reach a specific depth, such as a 90-degrees of depth, subject-specific depth, or largest possible depth [19]. In addition, a lot of research targets the eccentric and concentric stages of CMJ for further analysis [20-22]. This type of CMJ research provided an analysis of critical information that could be used by scientists and trainers to evaluate capabilities and expertise [22]. Athletes usually undergo neuromuscular training to achieve higher jumps and better physical conditioning, through strengthening the muscles and increasing the force applied during the propulsion phase [19, 22].

To enhance jump performance, athletes tend to apply a larger force, alter the duration of the force application, or squat at different depths [19]. Squatting at a specific depth during a CMJ can affect the duration of the jump and the peak forces in the propulsion phase, thus affecting the height of the jump [19]. With a longer depth in squatting, higher jumps are achievable at a shorter duration of time [19]. It has been shown previously, both in an experiment and in simulation, that increasing the countermovement depth can lead to better jump performance [19]. On the other hand, decreasing the depth does not allow enough energy to be stored in the muscles for the jump, and thus the jumping performance is compromised [19].

Overall, CMJ is a great tool to assess athletes' lower extremities, the power that can be applied, and to track capabilities. It has the potential of being used to evaluate injuries in the lower extremity, without the burden of intent to jump or the effect of arm swings.

2.2 Inverse Dynamics vs. Forward Dynamics

Human movements can be described as the motion of a system of rigid linked segments. This system is usually driven by internal or external forces that affect the dynamics. Simulations of this system are usually constructed in two directions, inverse dynamics or forward dynamics. Inverse dynamics is the process of obtaining internal forces and moments from kinematics and external forces [23]. Forward dynamics is the process of obtaining the movement and external reaction forces from known internal forces and moments [23]. Figure 3 shows an overflow of the inverse dynamics problem, where motion and external forces are the inputs, and the outputs are the internal forces and moments. Figure 4 shows an overflow of the forward dynamics problem, where joint torques and internal forces are the inputs, and the outputs are an estimation of the motion and external forces.

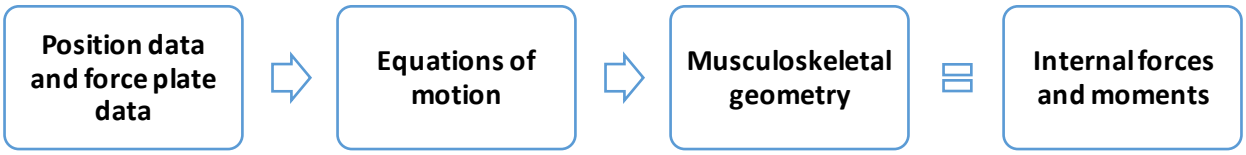

Figure 3: Flow chart of the inverse dynamics problem

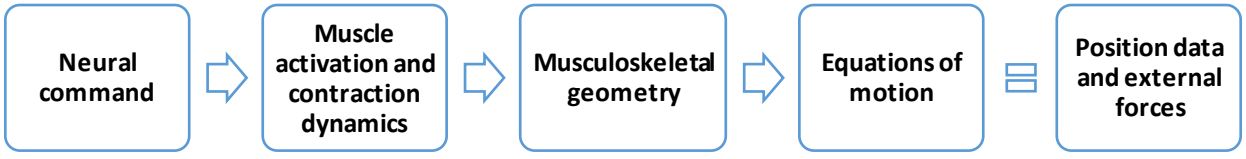

Figure 4: Flow chart of the forward dynamics problem

A typical inverse dynamics problem tackles the need of solving for joint torques. By using a simulated model, position data and ground reaction forces can be captured directly with motion capture systems and force plates, respectively. This method allows the calculation of internal forces and moments without invasive procedures, such as using pressure plates and dynamometry [23]. However, errors in capturing data and uncertainty in simulated model parameters can affect the consistency and accuracy of joint torques and forces obtained [24]. Inverse dynamics utilizes Newton-Euler equations of motion to obtain internal forces and moments about joints, through utilizing inertial properties of the rigid bodies, the kinematics of the motion, and external forces (ground reaction forces) [23]. A typical forward dynamics problem tackles the need of estimating the motion, through utilizing joint torques and internal forces (muscle forces) as inputs. This method allows computational prediction of motion under various conditions, without the need for an extensive amount of experimental data or experimental data of dangerous motions [25].

In sports, simulated models are utilized to give insight regarding the techniques used and to provide mechanics for better performance [26]. Analyzing the biomechanics of sports through the kinematics can provide an understanding of the techniques used. However, utilizing a simulated model can test several factors that affect the mechanics of the sport and can quantifiably provide information to improve the techniques to be used [26]. In addition, it can analyze the dynamics that can lead to a higher risk of injuries in sports, along with the possibility of studying subject-specific simulated models with unique factors that result in a specific motion [26].

2.3 Stress Fractures in Sports

Under repetitive impact loading of a bone, simple or complete fractures can take place [27]. Particularly, stress fractures are common with damage that takes place with high stresses that are constantly induced to the bone [27]. A stress fracture is also considered an overuse injury. As the bone is repeatedly loaded with high impactful forces, the bone experiences microdamage that increases in severity with a higher frequency or magnitude of loading [12]. Under repetitive high loads, the bone has the capability of remodeling [27]. This is that the bone can accommodate to the high frequency of larger loads by creating more bone cells and increasing the strength of the bone [12]. In addition, the bone is capable of regenerating bone cells to replace damaged cells prior to it escalating to a bone fracture [12]. However, enough time is required for the bone to remodel and accommodate to these high loads [27]. With stress fractures, each loading cycle induces microdamage in the bone [27]. With a high frequency of loading, bone damage can take place faster than bone remodeling, and thus stress fractures can occur [27]. In some cases, stress fractures are very hard to diagnose, even with well-developed imaging techniques [12]. In other cases, stress fractures can be severe and may require surgical intervention [12].

Several sports impose high impactful loads on the bones, such as basketball, volleyball, football, dancing, hockey, etc. Stress fractures can be detrimental to athletes as they can lead to weeks without strenuous activities until recovery is ensured [27]. In addition, athletes usually require rehabilitation to increase the strength of the bone after recovery to avoid the occurrence of a subsequent stress fracture [27].

Stress fractures account for up to 20% of all sports-related injures [27]. Stress fractures are more common in the bones of the lower extremity, such as the tibia and metatarsal, and less common in bones of the upper extremity [27]. In a study that examined stress fractures in 320 athletes of different sports, about 49.1% of all cases occurred in the tibia [28]. In addition, the site of fracture is possibly correlated to age, such that older individuals are more likely to experience stress fractures in the femur or the metatarsal, while younger individuals are more likely to experience stress fractures in the tibia or the fibula [28]. Due to the high prevalence of stress fractures in sports, a motivation existed to provide a better framework to understand stress fractures.

2.4 Merging of Multibody Dynamic Modeling and Finite Element Modeling

This section summarizes several research studies that tackled multibody biomechanical modeling and finite element modeling for the same problem. Computational modeling has been used vastly in the area of human biomechanics. Multibody modeling has been used when physical motion and dynamics are of interest. On the other hand, finite element modeling has been used when tissue response is of interest. Sometimes, analyzing both areas of biomechanics can provide important insight into a problem. Thus, research is slowly gearing towards the use of both a multibody dynamic model of the body and a finite element model of a tissue to tackle some problems in the field of biomechanics.

One study that tackled combining both computational models was the work of Alti et al. [29]. This work investigated the possibility of predicting the femoral neck strain during walking by utilizing multibody dynamic modeling and finite element modeling [29]. The goal of the work was similar to the goal of this thesis, which was to study the motion itself and study its effects directly on the femur [29]. It consisted of obtaining CT and MRI scans of the lower limb, along with data collection of the normal gait from five female participants [29]. These were used to create subject-specific multibody musculoskeletal models and subject-specific finite element models to investigate femoral neck strain values during gait [29]. Muscle forces that were obtained from the multibody model and optimization were used for boundary and loading conditions in the finite element model [29]. This work was able to provide multiple subject-specific models, along with comparing the sensitivity of the model to different inputs [29].

Another study by Xu et al. examined the effects of load carriage on the tibia by utilizing both a multibody model and a finite element model [4]. The goal of this work was to add to previous studies of motion by examining the stress and strain distribution of the tibia [4]. To add to that, a primary goal was to conduct finite element modeling under meaningful and accurate loading conditions [4]. This work consisted of obtaining motion data and ground reaction forces during walking with four conditions of carrying loads [4]. This data was utilized in a multibody dynamic model to obtain joint and muscle forces, which were applied as inputs for the finite element model of the tibial bone [4]. Overall, this work provided a framework that connects load carriage and biomechanics of bone [4].

Mo et al. also contributed to this framework by combining multibody modeling and finite element modeling simultaneously, through the use of controlling strategies [30]. This work incorporated "a unique feedback control strategy that couples together a basic Proportional-Integration-Differentiation (PID) controller and generic active signals from computed muscle control (CMC) method of the musculoskeletal model" [30]. It is considered the first step towards the possibility of simultaneously simulating dynamics of the motion and stress analysis of tissue [30].

Lastly, Shu et al. attempted to utilize a multibody dynamic model and a finite element model to tackle the full response of the body after a total knee replacement surgery [31]. The aim of this work was to examine the dynamics of the motion after the surgery and the prosthetic mechanics and structure, along with the interaction between them [31]. The multibody model incorporated a subject-specific knee model, ligaments, muscles, and a deformable prosthetic model [30]. This method allowed a more realistic analysis of the prosthesis model, by providing subject-specific boundary and loading conditions [31].

All this previous work helped shape the work presented in this thesis. This body of research allowed the development of a framework that fully captures the dynamics and tissue response of the human body during a full CMJ. This project aims to provide better insight towards examining impactful motions that are correlated to a higher risk of injuries.

Chapter 3

3 Construction of a Multibody Biomechanical Model

A multibpody biomechanical model of a human body during countermovement jumping was constructed in MapleSim (MapleSoft, Canada). The model is a two-dimensional representation that focuses on the motion of the lower extremity of the body. Experimental data were obtained for the motion of CMJ, followed by kinematic and kinetic analysis of this data to be used in creating the model. All the steps are explained in this chapter.

3.1 Experimental Data Collection

The experimental data consisted of tracking position data and gathering ground reaction forces during the motion of a CMJ. A healthy participant, male (23 years, 1.788 m, 80.5 kg), performed a set of required motions to obtain the experimental data.

To prepare the participant for the experiment, four marker clusters were attached as following: one cluster of four markers on the right thigh, a cluster of four markers on the right shank, a cluster of four markers on the right foot, and a cluster of five markers affixed over the sacrum of the pelvis. In addition, digitized points were selected to calibrate the system and obtain anatomically relevant position data as virtual markers. Digitized points included: left & right anterior superior iliac spines, left & right posterior superior iliac spines, left & right iliac crests of the pelvis, the sacrum, the right greater trochanter, the right medial and lateral femoral condyles and tibial condyles, the right medial and lateral malleolus, and the right heel, toe, first and fifth metatarsal of the foot.

The position of the markers was captured using six Optotrak Certus cameras (Northem Digital Inc., Canada), set at a capture frequency of 100 Hz. To capture ground reaction forces, 2 AMTI OR6-7 force plates were utilized at a capture frequency of 2000 Hz. Overall, the experimental procedure consisted of a static standing trial and 3 CMJ trials. The data collection started after attaching and digitizing markers, along with giving instructions and obtaining consent from the participant. At first, the participant was asked to stand still on the force plate for a duration of 3 seconds. This is the static standing trial, required for calibration and to help in defining the

weight of the subject. The participant is then asked to perform a CMJ, with hands still on the waist, to reach the maximum height attainable. The duration of the trial was set to 30 seconds to allow the participant to prepare for the second trial and to reduce the effect of fatigue or rapidness of continuous jumping. The two remaining trails followed similarly to trial 1. Upon completing the three trials of CMJ, the markers were removed, and the experimental procedure was concluded.

The Office of Research Ethics at the University of Waterloo approved the experimental procedure (ORE #31448) and consent to the study was provided by the participant. This experiment was performed by Natasha Ivanochko at the University of Waterloo.

3.2 Analysis of Experimental Kinematics

Upon gathering the position data of CMJ, an inverse kinematic analysis was conducted in MATLAB. At first, the data was filtered to remove noise and gap filled to estimate the position of missing markers at a specific frame. Joint centers (hip, knee, and ankle) were specified based on ISB recommendations of the lower extremity [32-33]. Then, a rotation matrix and local coordinates of the lower extremity segments were utilized to obtain joint angles.

To explain the motion in an anatomically relative aspect, intersegmental angles were computed and Figure 5 shows the convention of joint angles utilized. Figure 6 depicts the plot of intersegmental angles of the thigh relative to the pelvis versus time. Figure 7 depicts the plot of intersegmental angles of the shank relative to the thigh versus time. Figure 8 depicts the plot of intersegmental angles of the foot relative to the shank versus time.

Intersegmental angles of the thigh relative to the pelvis corresponds to the angles of the hip joint, shank relative to the thigh corresponds to the angles of the knee joint, and foot relative to the shank corresponds to the angles of the ankle joint. Based on the rotation matrix selected for this motion, alpha (α) angles correspond to the abduction-adduction motion of joints. Beta (β) angles correspond to the internal-external rotation of joints. Moreover, gamma (γ) angles correspond to the flexion-extension motion of joints.

By examining the intersegmental angles, majority of the motion takes place in flexion and extension of the joints of the lower extremity, which corresponds to most of the motion being in the sagittal plane. Flexion-extension angles of the ankle joint reach a maximum of -35° for both jumping and landing. Flexion-extension angles of the knee joint reach a maximum of 84° for jumping and around 59° for landing. Moreover, flexion-extension angles of the hip joint reach a maximum of -105° for jumping and about -44° for landing.

Figure 5: Convention of the angles obtained from experimental data of countermovement jumping

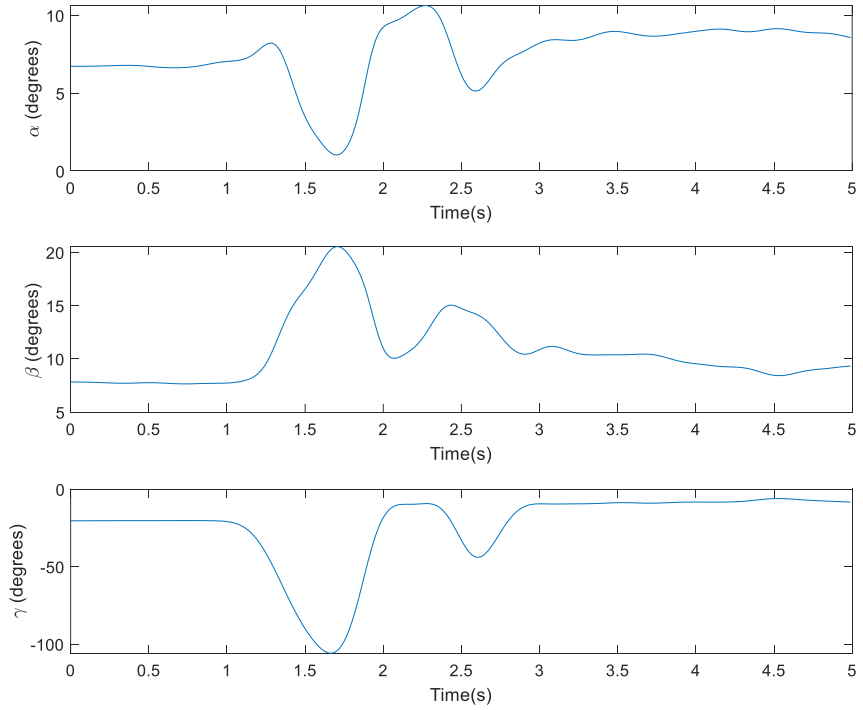

Figure 6: Intersegmental angle of the thigh relative to the pelvis (hip joint) during a CMJ task

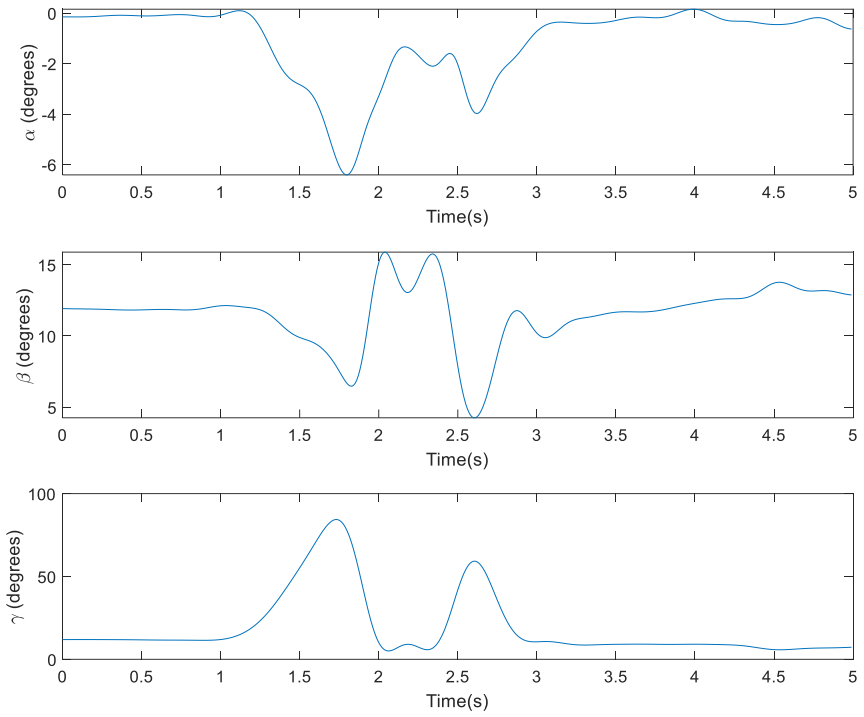

Figure 7: Intersegmental angle of the shank relative to the thigh (knee joint) during a CMJ task

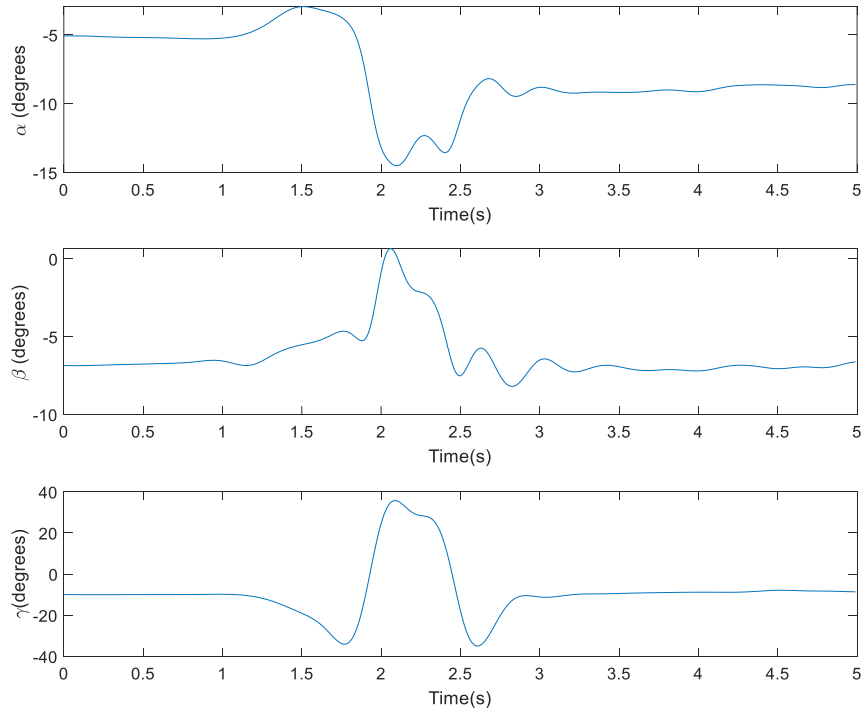

Figure 8: Intersegmental angle of the foot relative to the shank (ankle joint) during a CMJ task

3.3 Analysis of Ground Reaction Forces

For the task studied, 2 force plates were active to fully capture the ground reaction forces during the entire motion. The force plate data obtained was calibrated in MATLAB to convert voltage data to ground reaction forces in Newtons. As recommended for impact loading tasks, the force plate data were filtered using the same cut-off frequency as the position data [34]. In addition, the data was utilized to obtain the center of pressure of contact throughout the motion, to be used phase IV of this work. Figure 9 shows a plot of the ground reaction forces in the vertical direction versus time for the three trials conducted, where ground reaction forces are normalized to the body weight of the participant.

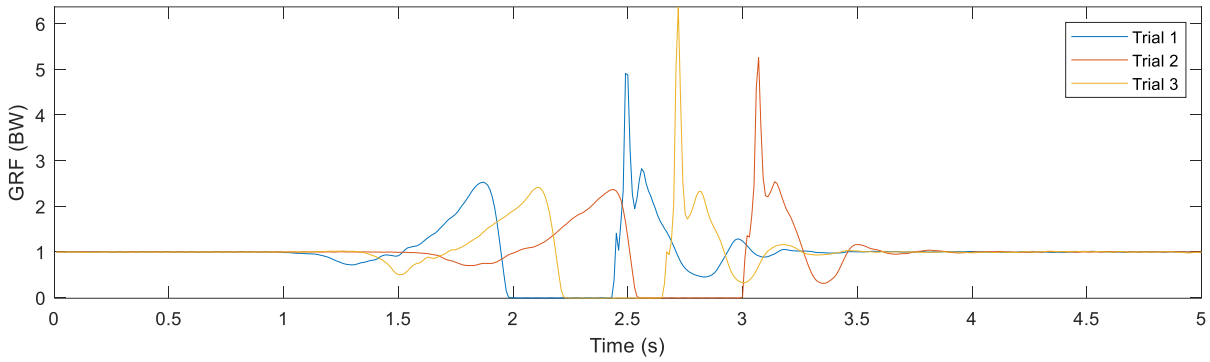

Figure 9: Vertical ground reaction force versus time for the three trials of CMJ task

Upon obtaining the ground reaction forces for the task of countermovement jumping, a comparison was made to understand the different stages of the task and how that correlates to the force. All three trials resulted in very similar patterns of ground reaction forces during a CMJ. The maximum GRF obtained during jumping was 2.4 ± 0.15 BW, while the maximum GRF obtained during landing was 5.60 ± 0.61 BW.

For further analysis, trial 1 was examined further. Figure 10 illustrates the different stages of the CMJ motion of trial 1. From 0 to 1 second, the subject is in a quiet stance, and the force plate measures the weight of the subject. This is referred to as the standing stage [21]. From 1 to 1.5 seconds, flexion of the hip and the knee takes place to reach the squatting position. This is referred to as the unweighting stage, where the ground reaction force drops below bodyweight [21]. Due to squatting, muscles store the energy required to attain the jump. From 1.5 to 2 seconds, the subject depicts the highest ground reaction force prior to flight. This is referred to as the

propulsion phase [21]. At 2 seconds, the subject's feet are off the ground and the force plate does not measure any force until around 2.4 seconds. The subject reaches a maximum height and drops back to touch the ground, and this is referred to as the flight stage [21]. At approximately 2.4 seconds, the feet touch the ground and force is detected again on the force plate. Just as the subject landed, a spike in the ground reaction force is observed. The GRF during landing is higher than that of propulsion. The subject then tries to reach a balance of standing upright, usually through squatting. The stage from 2.4 to 3.2 seconds is referred to as the landing phase [21]. This is then followed again by a standing phase, where balance is achieved. Similar patterns and ranges of GRFs are observed in previous literature [20, 22]. All the stages are explained further in section 2.2.

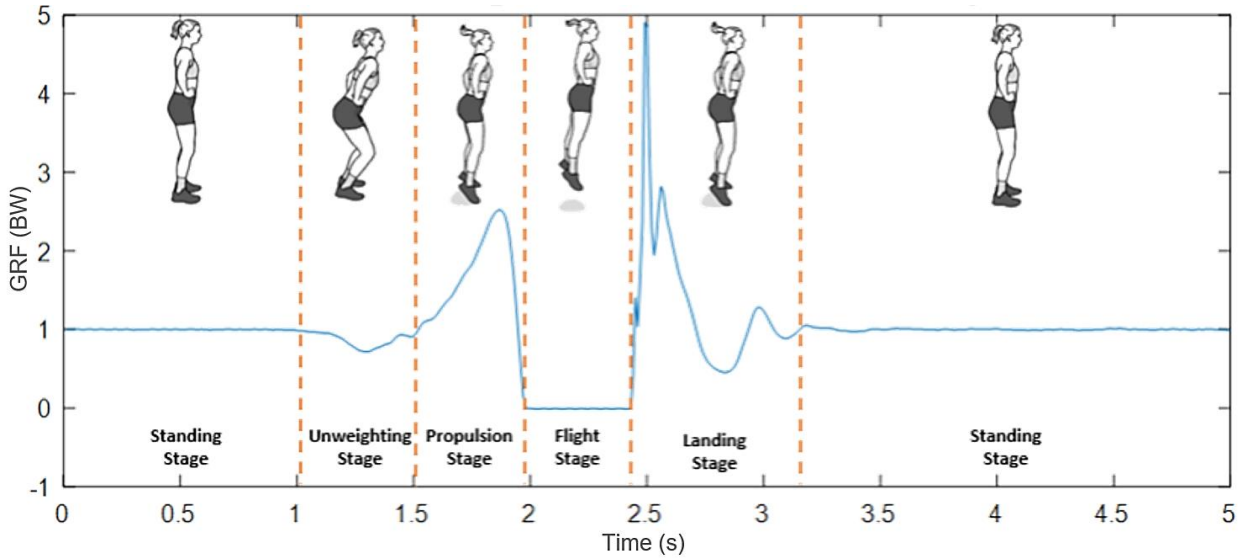

Figure 10: Illustration of the different stages of CMJ with respect to the vertical ground reaction forces of trial 1

3.4 Design of Biomechanical Model

The purpose of this step was to design a biomechanical computational model with all the body segments that are critical for the motion studied. In other words, it is a simplified mathematical model of the body that can capture the motion of interest. In this study, it has been assumed that a sagittal plane analysis is adequate, rather than a 3D analysis. The motion mainly involves flexion and extension of joints, with minimal motion in internal/external rotation and abduction/adduction of joint (change of <15°). In addition, the model is assumed to be symmetrical. This assumption is made due to very similar motions depicted for both the right side and left side of the body. It must be noted that the body dominance of one side of the body was not investigated in this project. Moreover, the biomechanics of the lower extremity is of interest and arm motion is restricted, thus the upper extremity was lumped to one segment.

A skeletal linked model was constructed in MapleSim to contain 4 rigid bodies and 3 revolute joints. The four rigid bodies consist of the foot, shank, thigh, and head-arm-trunk (HAT). For a 2D model, left and right bodies are lumped into a single segment (i.e. left and right thighs are lumped into one thigh segment). A simple schematic is shown in Figure 11. Revolute joints were used for the hip, knee, and ankle joint to drive the model. Based on the subject's height and weight, important properties and parameters required for the model were obtained by anthropometric scaling factors found in the literature [35]. This includes segmental length, mass, center of mass location and moment of inertia for HAT, thigh, shank, and foot segments.

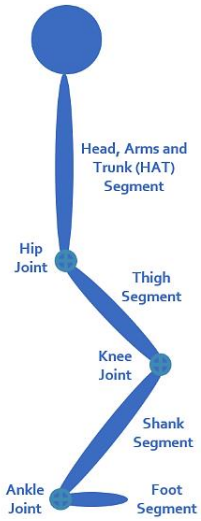

Figure 11: Illustration depicting the segments and joints of the dynamic multibody model

Chapter 4

4 Dynamic Simulations

This chapter covers phase IV, tackling the implementation of an inverse dynamic analysis for countermovement jumping. For this study, a biomechanical model was constructed (section 3.4), and was utilized with kinematic and kinetic data to obtain joint torques and reaction forces.

4.1 Dynamics of a Countermovement Jump

Inverse dynamic analysis was conducted using the skeletal model generated in MapleSim. The model was employed to obtain internal joint forces and joint moments of the lower extremity. The model was constructed with subject-specific weights and lengths for each segment, moment of inertia for each segment, and the center of mass of each segment. As inputs to the model for the inverse dynamic analysis, intersegmental angles of the hip, knee, and ankle were added to the model. In addition, ground reaction forces were applied to the foot segment at the average center of pressure for every stage of the countermovement jump. In addition, horizontal and vertical position data of the hip joint (pelvis) were applied to the model. These inputs provided enough information to conduct an inverse dynamic analysis. The desired output of this analysis was the sagittal joint moments of the hip, knee, and ankle joints, along with knee and ankle joint contact forces. In MapleSim, the multibody analysis tool was utilized to obtain the motion dynamics, based on the Newton-Euler equations of motions.

4.2 Simulations of Inverse Dynamics

By conducting an inverse dynamic simulation, Figure 12 shows the resultant hip, knee, and ankle joint moments obtained during the task of countermovement jumping. During the propulsion phase, peak moments obtained were -300 N.m for the hip joint moment, 222 N.m for the knee joint moment, and -87 N.m for the ankle joint moment. During the landing phase, the highest moments obtained were -329 N.m for the hip joint moment, 271 N.m for the knee joint moment, and -169 N.m for the ankle joint moment. The peak joint moments obtained in this analysis correlated with previously reported joint moments during the task of vertical jumping (-350 N.m for the hip joint moment, 188 N.m for the knee joint moment, and -110 N.m for the ankle joint moment) [36].

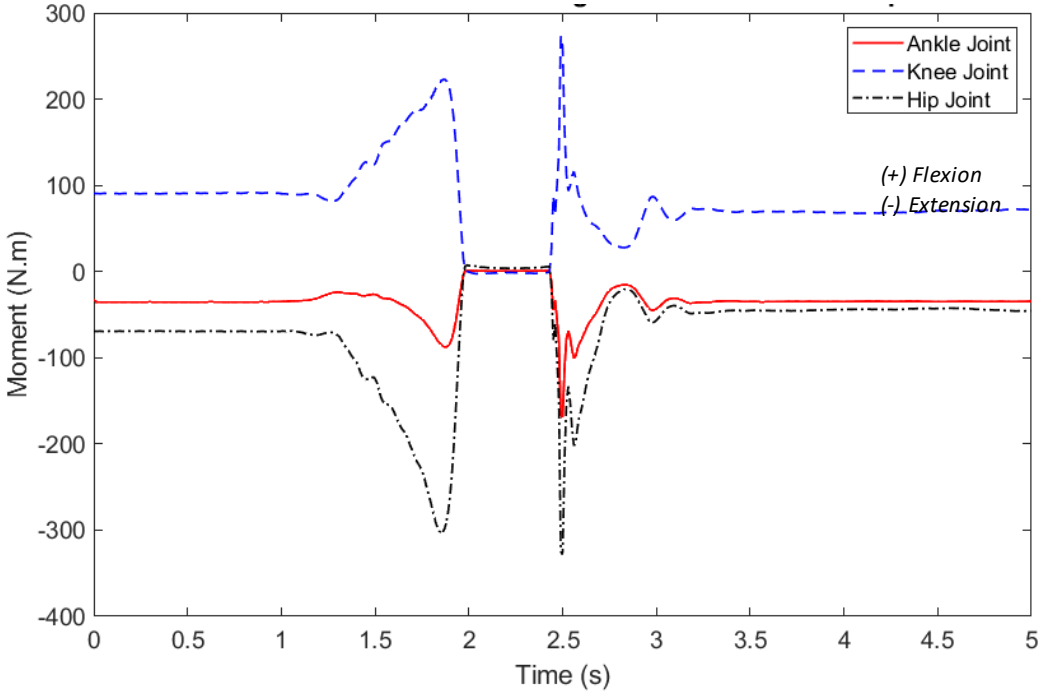

Figure 12: Flexion/extension joint torques of the hip, knee, and ankle joint during a CMJ

Other outputs that were achieved from the biomechanical model are the joint contact forces of the knee and the ankle joint. Figure 13 shows a simplified free body diagram of the reaction forces. Figure 14 shows the horizontal and vertical joint contact forces of the knee during the motion of CMJ. Figure 15 shows the horizontal and vertical joint contact forces of the ankle during the motion of CMJ. Vertical forces were normalized to the bodyweight of the subject to be easily correlated to GRFs. The maximum vertical knee joint contact force was achieved during the landing stage of the motion, with a maximum force of approximately -1797 N. During jumping, the maximum knee joint contact force was approximately -878 N. To add to that, the maximum vertical ankle joint contact force was achieved during the landing stage of the motion, with a maximum force of approximately 1850 N. During jumping, the maximum ankle joint contact force was approximately 813 N. The peak vertical reaction forces of the ankle closely match to half of the peak ground reaction forces measured experimentally. The vertical reaction forces correlated closely to literature during countermovement jumping, which showed maximum knee and ankle joint contact forces of -1622 N and 1699 N, respectively [5]. In addition, the overall response and pattern of the joint contact forces during the full motion closely resembles that of previous literature [7]. To verify of the results, the equations of motion of the model were extracted from MapleSim and verified the solver in MATLAB with the same inputs.

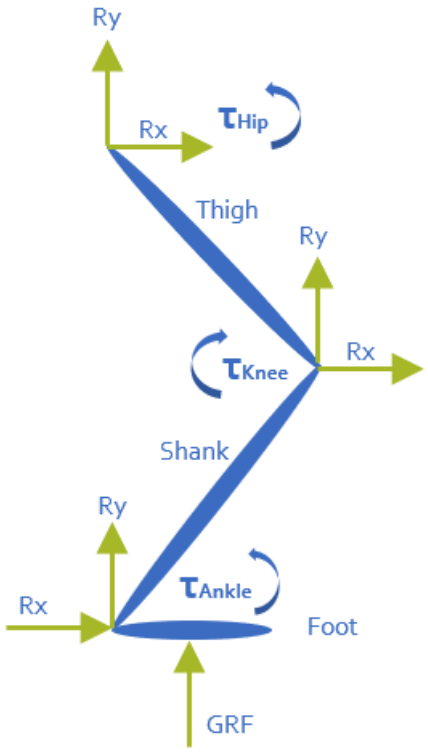

Figure 13: A simplified free body diagram of the lower extremity to depict the reaction forces

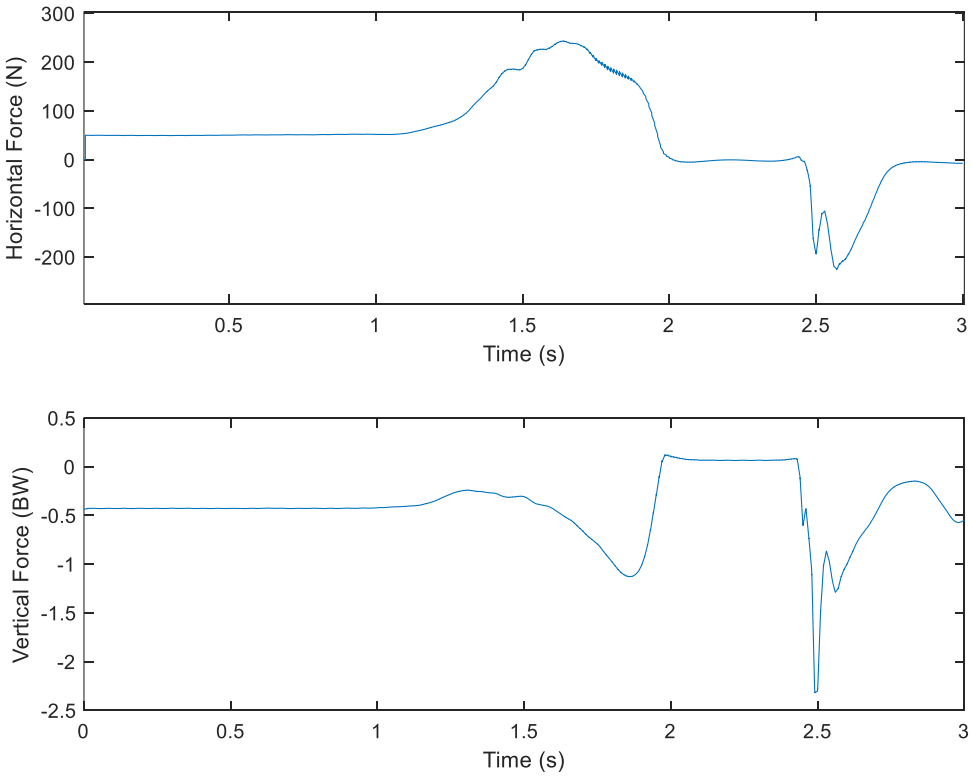

Figure 14: Horizontal and vertical joint contact forces of a knee during CMJ

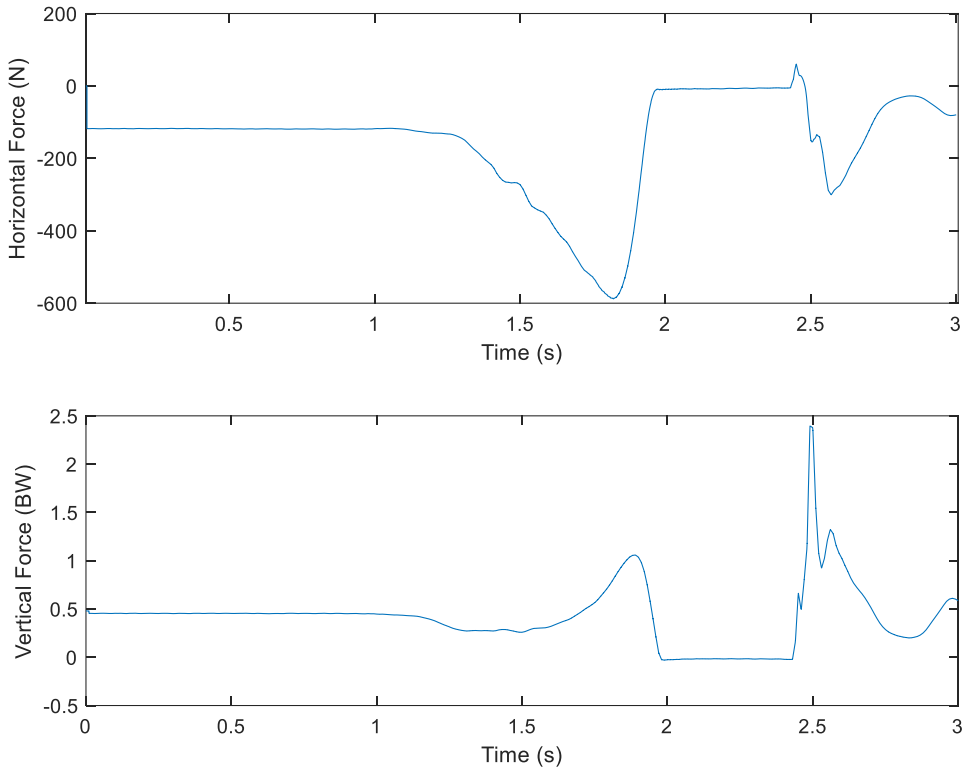

Figure 15: Horizontal and vertical joint contact forces of an ankle during CMJ

Chapter 5

5 Muscle Forces

This chapter covers phase V of this project, tackling the problem of obtaining muscle forces during a CMJ from joint torques obtained in phase IV of this work. For this study, muscles that are attached to the tibia are of main interest, as these muscle forces will be needed as inputs to the finite element model. Static optimization was used to solve for muscle forces through minimizing a specified objective function. A numerical and an analytical approach were used for static optimization, described respectively in sections 5.2 and 5.3.

5.1 Static Optimization Solution for Redundant Muscle Forces

By utilizing the output of the MapleSim model in phase IV, the next aim of this project was to find the forces generated by several muscles in the lower extremity. In the attempt of solving for the muscle forces, the problem of redundancy was faced. This occurs when the number of unknowns in the problem is larger than the number of equations generated from the model. With the muscles recruited in this model and the associated degrees of freedom, muscle forces can not be obtained directly [35]. To tackle this, an optimization problem can be used. Static optimization in inverse dynamics is an approach to estimate the muscle forces for every time instant in the motion [37]. This is one of the most used methods in inverse dynamics to solve the problem of redundancy of muscle forces [37]. The static optimization utilizes an objective function that is minimized while depicting some physiological characteristics [38].

To conduct a static optimization, additional inputs are required. Thus, the multibody dynamic model is upgraded from a skeletal model to a musculoskeletal model. Several muscles were added to the model, with a focus on muscles that are attached to the tibia. For this project, a total of 9 muscle bundles were examined. This includes the gluteus maximus muscle, iliacus muscle, rectus femoris muscle, hamstring muscle (which is composed of bicep femoris long head, semimembranosus, and semitendinosus), vasti muscle, biceps femoris short head muscle, gastrocnemius muscle, soleus muscle, and tibialis anterior muscle.

Musculoskeletal geometry was incorporated in this model by obtaining the site of muscle attachments, via points of muscles, moment arms, and muscle lines of action. Location of muscle insertion, muscle origin, and via points around joints were obtained using the Klein Horsman's database [39]. In addition, optimal moment arms and muscle lines of action were obtained using data from Yamaguchi [40]. A scale factor of 1.076 was used to match the positions and lengths of the subject in this study to that in the databases.

It is first assumed that the moments about the joints are only due to muscle forces [41]. In addition, muscle dynamics were not incorporated and thus it is assumed that muscles can produce force instantly. A variety of objective functions have been utilized in obtaining muscle forces, but the focus was mainly towards polynomial functions [41]. A commonly used objective function of muscle stresses is based on the work of Crowninshield, giving the following criterion [38]:

$$minimize \sum_{i=1}^{n} \left(\frac{F_i}{PCSA_i}\right)^p \quad (1)$$

where n is the number of muscles about the joint studied, F_i is the i^{th} muscle force, $PCSA_i$ is the physiological cross-sectional area of the i^{th} muscle and p is the power of the criterion. The power of the criterion is greatly variable in the literature, where some are random to better fit the experimental results, while others aim for physiologically meaningful criteria [41, 42]. Several pieces of research conducted analysis for the effects of changing the power of the criterion in static optimization [43, 44]. For this project, the power was varied, with emphasis on the power of 3, which resembles maximizing of energy expenditure and is very widely used in literature [42]. Another commonly used objective function is based on relative muscle forces [45]. It is based on the following criterion:

$$minimize \sum_{i=1}^{n} \left(\frac{F_i}{F_{i\_max}}\right)^p \quad (2)$$

where F_{i_max} is the maximum isometric force of the i^{th} muscle. Both objective functions incorporate physiological criteria of the muscles, but the muscle forces are usually different [45]. For this project, the objective function of relative muscle forces (equation 2) was used with varying powers, to be compared to the objective function of muscle stresses (equation 1).

A flow chart of the static optimization problem is illustrated in Figure 16. It shows that joint moments and muscle moment arms from the musculoskeletal model can be used with maximum isometric muscle forces and physiological cross-sectional area of muscle to run a static optimization problem. The aim of this optimization is to obtain optimal muscle forces for a CMJ motion.

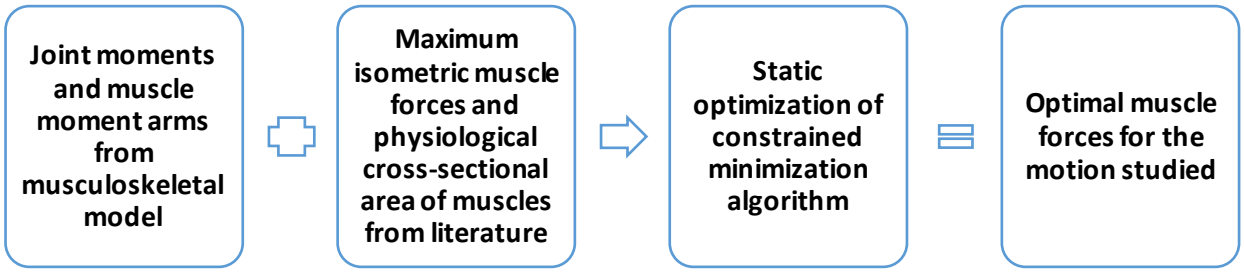

Figure 16: Flowchart of the static optimization problem to solve for muscle redundancy

The problem of static optimization was solved for each joint, where the input is the total moment of the joint. This means that the summation of muscle moments should be equal to the total moment. The values of maximum force and physiological cross-sectional area were obtained from literature [46-48]. An analytical approach and a numerical approach were used to obtain muscle forces. In the static optimization problem, equality and inequality constraints were set to bound the muscle forces and obtain meaningful results. For all static optimization problems in this project, the same set of constraints were utilized as follows:

$$Inequality\ Contraint \quad F_i \leq F_{i\_max} \tag{3}$$

$$Inequality\ Contraint \quad F_i \geq 0 \tag{4}$$

$$Equality\ Contraint \quad \tau_{joint} - \sum_{i=1}^{n} r_i F_i = 0 \tag{5}$$

where r_i is the moment arm of the i^{th} muscle, and τ_{joint} is the total joint moment. The inequality constraints bound the problem to ensure all muscle forces are positive and are lower than their maximum isometric forces. The equality constraint in this problem is to ensure that the joint moment obtained from the musculoskeletal model is equal to the net muscle moments obtained from the results of the static optimization.

5.2 Numerical Approach

To solve the problem of static optimization, the fmincon function in the optimization toolbox of MATLAB was used. A code was generated in MATLAB to tackle the problem of muscle redundancy for a CMJ. The algorithm solves a constrained minimization problem to compute optimal muscle forces. The fmincon function requires the inputs of the static optimization to be applied in a specified format as following:

$$Minimize\ f(x)\ such\ that\ \begin{cases} Aeq\ .x = beq \\ lb \leq x \leq ub \end{cases} \tag{6}$$

$$Where\ \begin{cases} f(x) = minimize\ \sum_{i=1}^{n} \left(\frac{F_i}{PCSA_i}\right)^p \\ Aeq = Moment\ arms\ of\ muscles \\ beq = Joint\ moment\ (inverse\ dynamics \\ lb = F_{i\_min} = 0 \\ ub = F_{i\_max} \end{cases} \tag{7}$$

Where *f(x)* is the objective function of the static optimization to obtain muscle forces, *Aeq* are the moment arms of muscles, *beq* is the joint moment, and *lb* and *ub* are the bounds of the muscle forces to meet inequality constraints. Overall, the function follows the representation of an optimization problem with equality and inequality constraints. All the inputs required for the objective functions and constraints were added to the code to generate a solution for the redundancy problem of muscle forces. For the initial guess of this optimization, the muscle forces at t=0 seconds obtained in the analytical approach of p=2 was used (to be explained in section 5.3). For this approach, the power of the objective function was varied to examine the effect of increasing the power. Thus, optimization was conducted for the power of 2, 3, 5, 10, and 20. Based on previous literature, increasing the power depicted higher synergy of muscles, i.e. more muscles contributing to net moment [41, 49].

The static optimization was conducted for the hip, knee, and ankle joint moments, along with muscles that cause the moments of each joint. It must be noted that only the main muscles were added to the analysis of this project.

For the ankle joint, Figure 17 to Figure 21 show the results of static optimization under different powers of the objective function. In addition, Table 1 shows the peak forces of muscles during the jumping and landing phase of the countermovement jump.

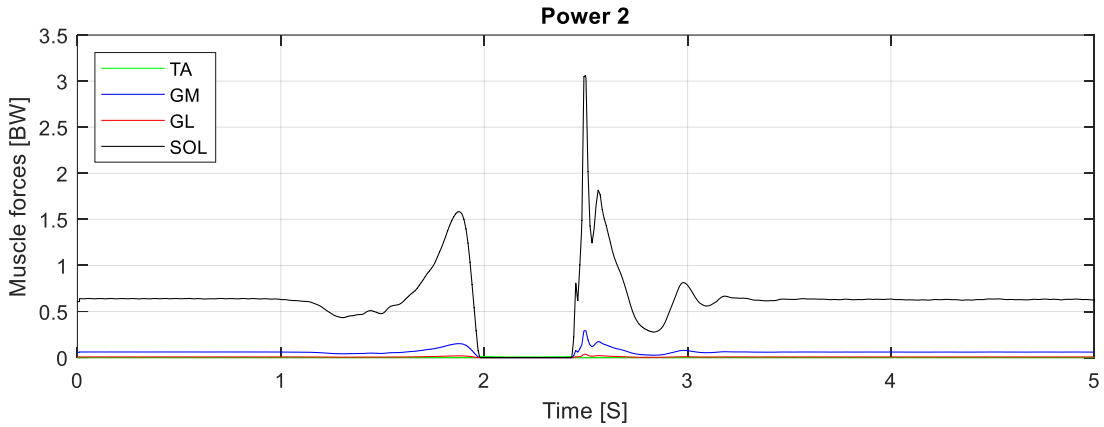

Figure 17: Numerical solution of muscle forces about the ankle joint with objective function of muscle stresses, p=2

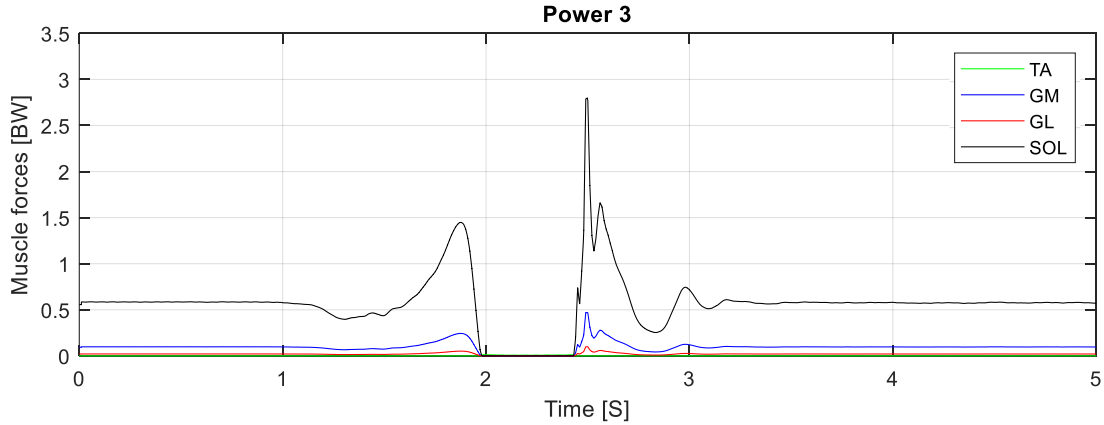

Figure 18: Numerical solution of muscle forces about the ankle joint with objective function of muscle stresses, p=3

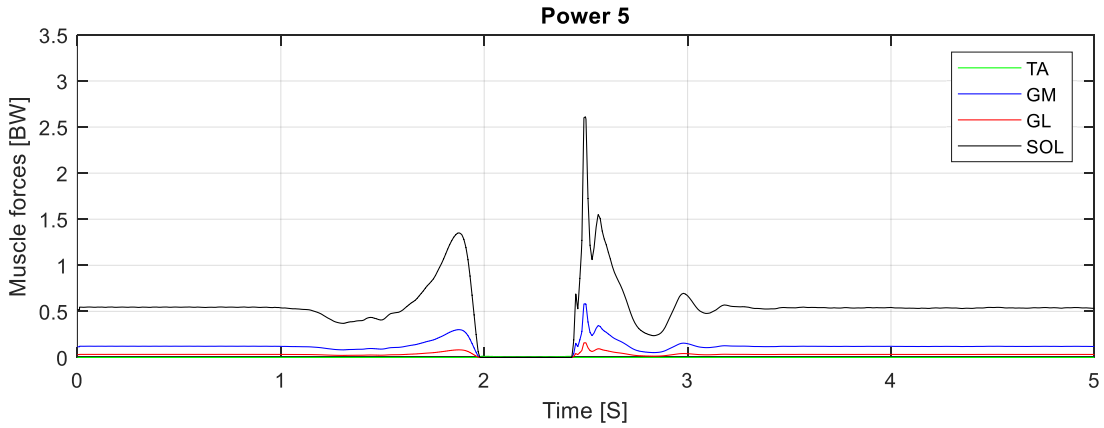

Figure 19: Numerical solution of muscle forces about the ankle joint with objective function of muscle stresses, p=5

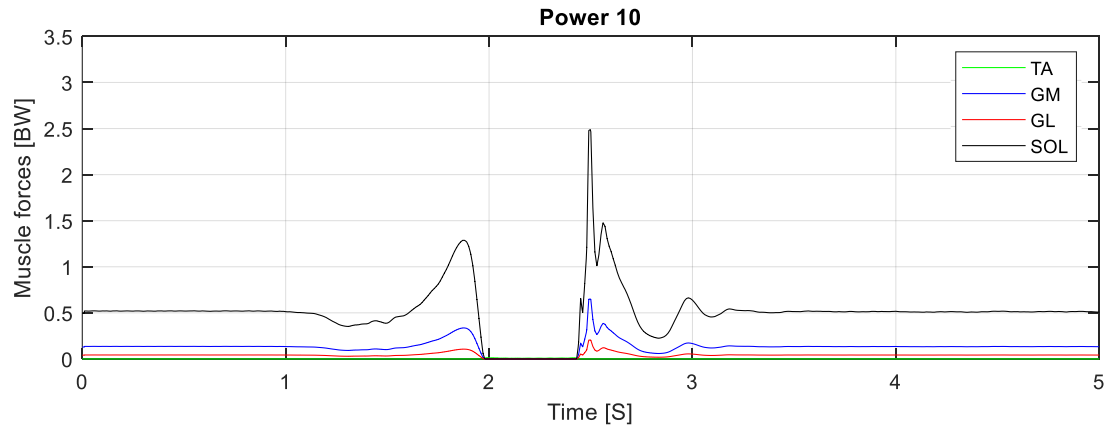

Figure 20: Numerical solution of muscle forces about the ankle joint with objective function of muscle stresses, p=10

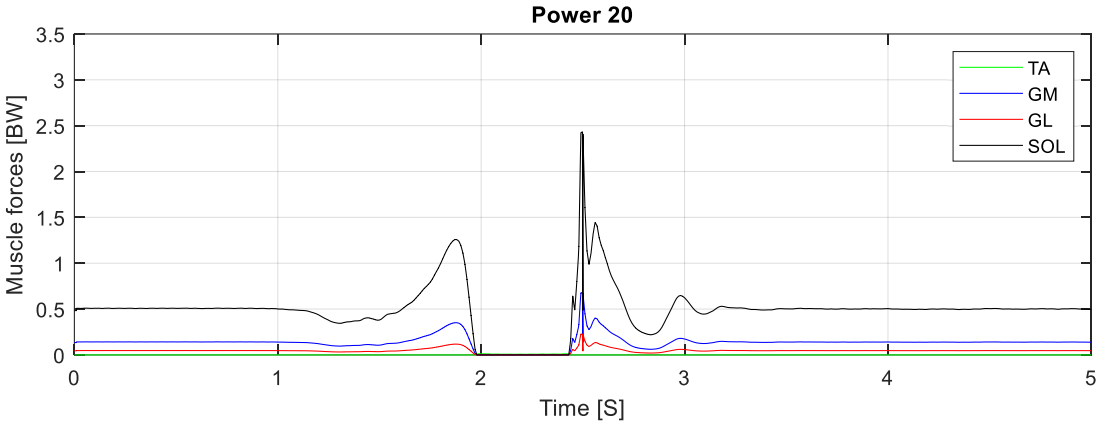

Figure 21: Numerical solution of muscle forces about the ankle joint with objective function of muscle stresses, p=20

Table 1: Peak forces of muscles about the ankle joint during jumping and landing of CMJ - numerical approach with objective function of minimizing muscle stresses to the power of 3, 10, and 20

Muscles Examined	Peak Jumping Force (p=3)	Peak Landing Force (p=3)	Peak Jumping Force (p=10)	Peak Landing Force (p=10)	Peak Jumping Force (p=20)	Peak Landing Force (p=20)
Soleus	1.447 BW	2.795 BW	1.279 BW	2.488 BW	1.258 BW	2.423 BW
Lateral Head of Gastrocnemius	0.051 BW	0.098 BW	0.106 BW	0.203 BW	0.117 BW	0.227 BW
Medial Head of Gastrocnemius	0.243 BW	0.466 BW	0.334 BW	0.644 BW	0.351 BW	0.676 BW

For the knee joint, Figure 22 to Figure 26 show the result of static optimization under different powers of the objective function of muscle stresses. In addition, Table 2 shows the peak forces of muscles during the jumping and landing phase of the countermovement jump.

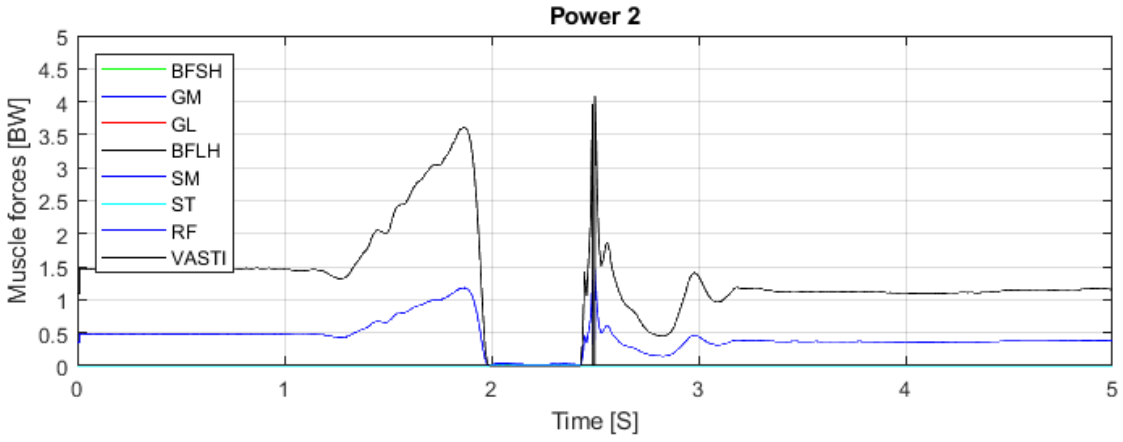

Figure 22: Numerical solution of muscle forces about the knee joint with objective function of muscle stresses, p=2

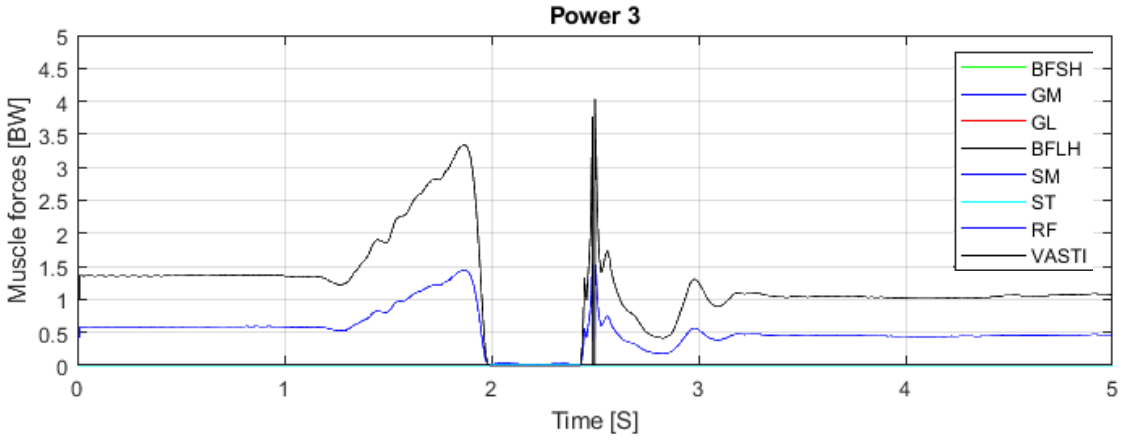

Figure 23: Numerical solution of muscle forces about the knee joint with objective function of muscle stresses, p=3

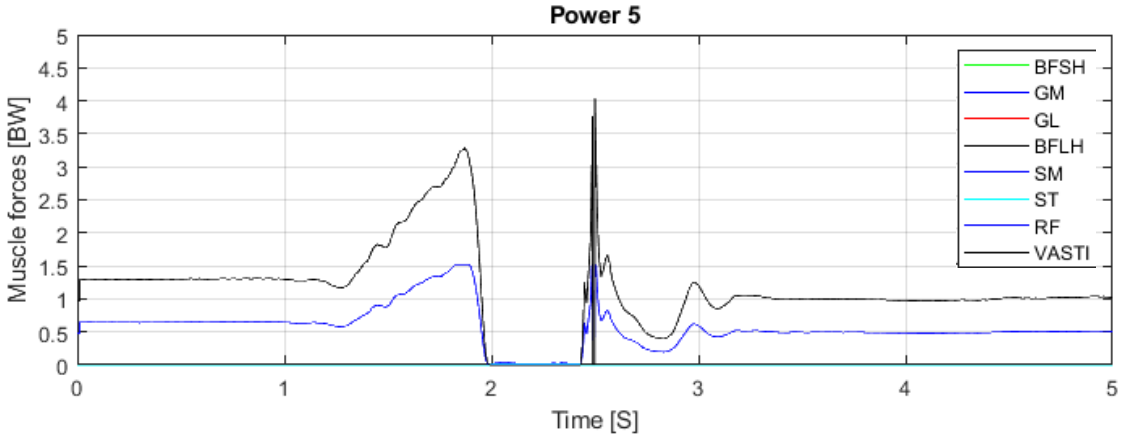

Figure 24: Numerical solution of muscle forces about the knee joint with objective function of muscle stresses, p=5

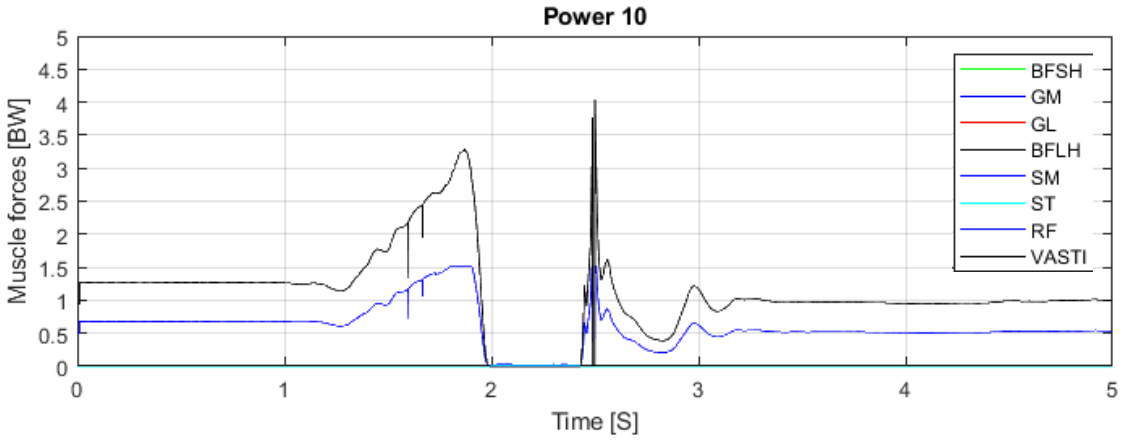

Figure 25: Numerical solution of muscle forces about the knee joint with objective function of muscle stresses, p=10

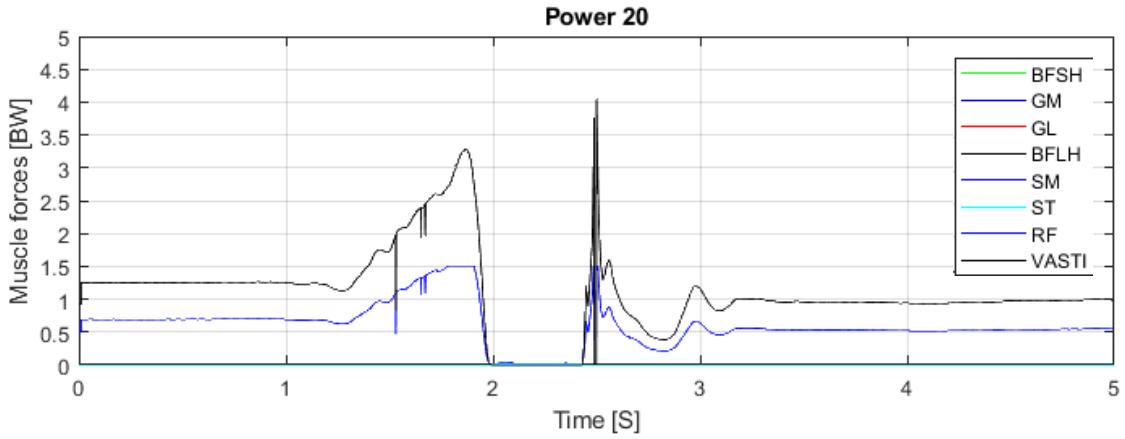

Figure 26: Numerical solution of muscle forces about the knee joint with objective function of muscle stresses, p=20

Table 2: Peak forces of muscles about the knee joint during jumping and landing of CMJ - numerical approach with objective function of minimizing muscle stresses to the power of 3, 10, and 20

Muscles Examined	**Peak Jumping Force (p=3)**	**Peak Landing Force (p=3)**	**Peak Jumping Force (p=10)**	**Peak Landing Force (p=10)**	**Peak Jumping Force (p=20)**	**Peak Landing Force (p=20)**
Vasti	3.349 BW	4.045 BW	3.277 BW	4.047 BW	3.271 BW	4.045 BW
Rectus Femoris	1.435 BW	1.49 BW	1.502 BW	1.506 BW	1.508 BW	1.508 BW

For the hip joint, Figure 27 to Figure 31 show the result of static optimization under different powers of the objective function of muscle stresses. In addition, Table 3 shows the peak forces of muscles during the jumping and landing phase of the countermovement jump.

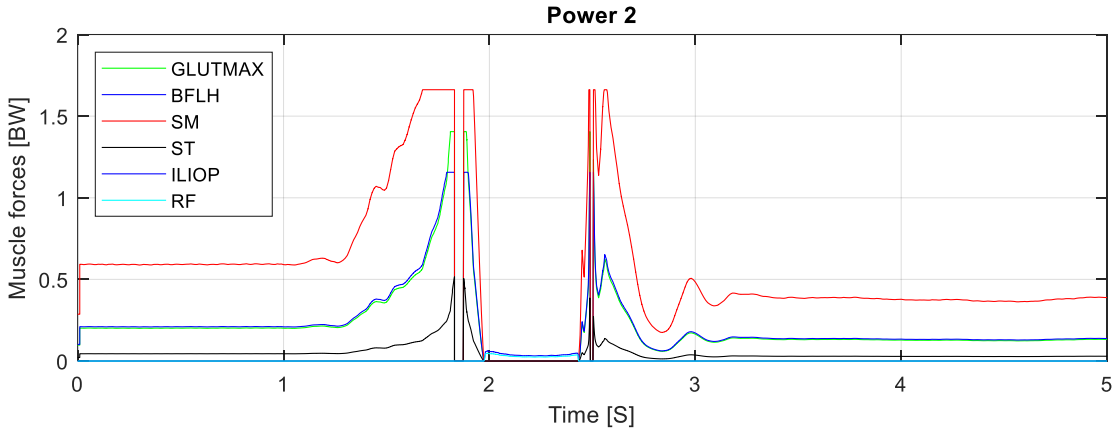

Figure 27: Numerical solution of muscle forces about the hip joint with objective function of muscle stresses, p=2

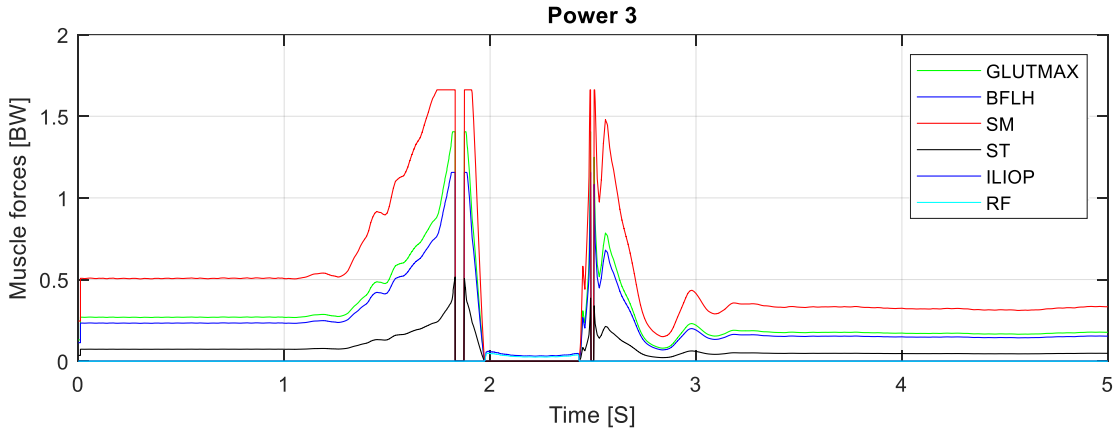

Figure 28: Numerical solution of muscle forces about the hip joint with objective function of muscle stresses, p=3

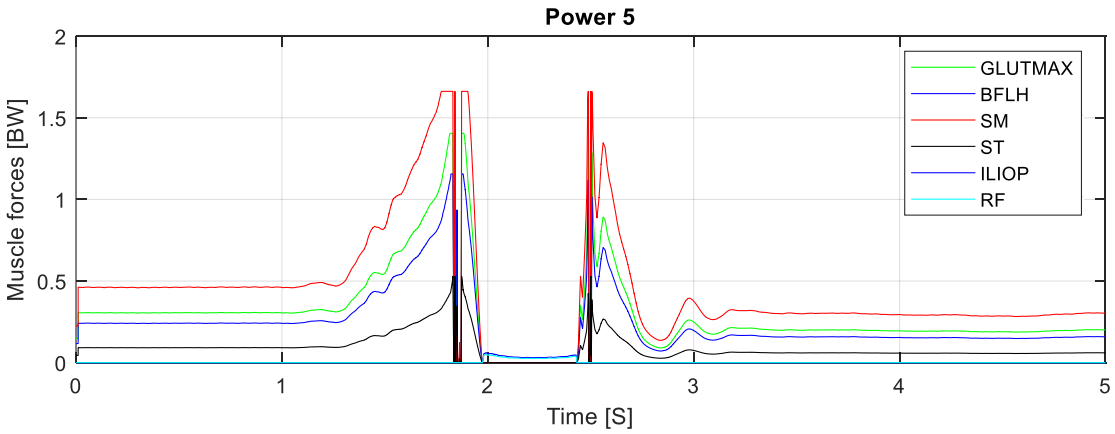

Figure 29: Numerical solution of muscle forces about the hip joint with objective function of muscle stresses, p=5

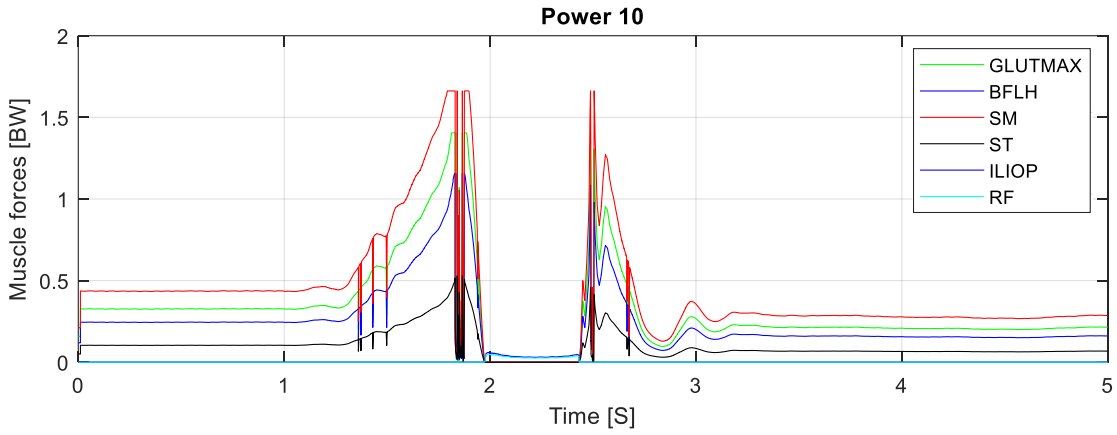

Figure 30: Numerical solution of muscle forces about the hip joint with objective function of muscle stresses, p=10

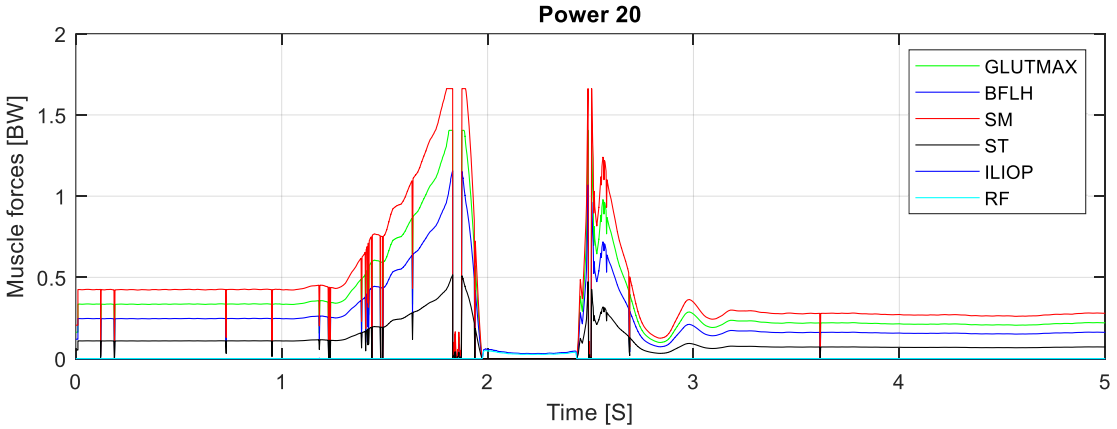

Figure 31: Numerical solution of muscle forces about the hip joint with objective function of muscle stresses, p=20

Table 3: Peak forces of muscles about the hip joint during jumping and landing of CMJ - numerical approach with objective function of minimizing muscle stresses to the power of 3, 10, and 20

Muscles Examined	Peak Jumping Force (p=3)	Peak Landing Force (p=3)	Peak Jumping Force (p=10)	Peak Landing Force (p=10)	Peak Jumping Force (p=20)	Peak Landing Force (p=20)
Gluteus Maximum	1.405 BW	1.249 BW	1.405 BW	1.405 BW	1.405 BW	1.405 BW
Bicep Femoris Long Head	1.156 BW	1.156 BW	1.156 BW	1.084 BW	1.156 BW	1.069 BW
Semimembranosus	1.622 BW	1.622 BW	1.622 BW	1.622 BW	1.622 BW	1.622 BW
Semitendinosus	0.498 BW	0.386 BW	0.516 BW	0.459 BW	0.516 BW	0.473 BW

With the numerical approach, it was of interest to investigate the effect of using a different objective function. Thus, the objective function of relative muscle forces was applied to compare the two objective functions. Similarly, the fmincon function requires the inputs of the static optimization to be applied in a specified format as following:

$$Minimize\ f(x)\ such\ that\ \begin{cases} Aeq\ .x = beq \\ lb \le x \le ub \end{cases} \tag{8}$$

$$Where\ \begin{cases} f(x) = minimize\ \sum_{i=1}^{n} \left(\frac{F_i}{F_{i\_max}}\right)^p \\ Aeq = Moment\ arms\ of\ muscles \\ beq = Joint\ moment \\ lb = F_{i\_min} = 0 \\ ub = F_{i\_max} \end{cases} \tag{9}$$

where f(x) is the objective function of the static optimization. For this optimization, only the muscles about the ankle joint were analyzed. For the initial guess of this optimization, the muscle forces at t=0 seconds obtained in the analytical approach of p=2 was used (to be explained in section 5.3). Figure 32 to Figure 36 show the result of static optimization under different powers of the objective function of muscle stresses. In addition, Table 4 shows the peak forces of muscles during the jumping and landing phase of the countermovement jump.

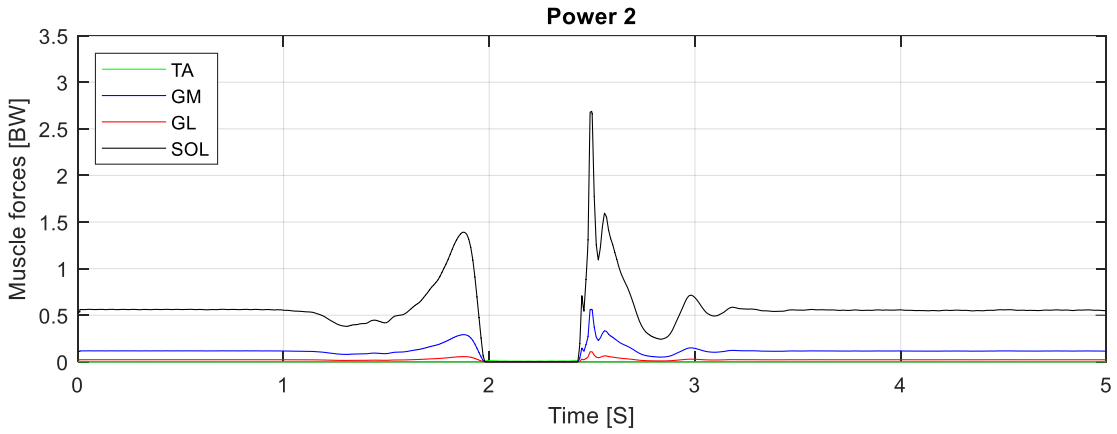

Figure 32: Numerical solution of muscle forces about the ankle joint with objective function of relative muscle forces, p=2

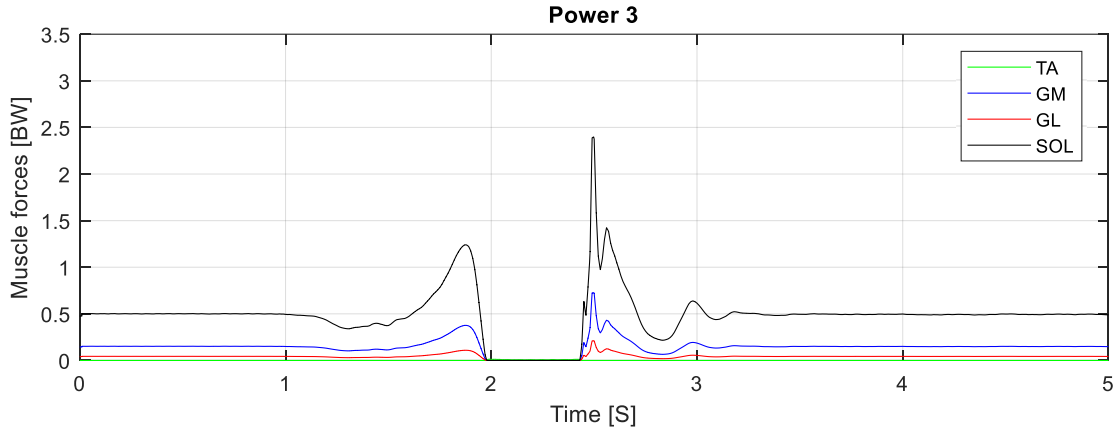

Figure 33: Numerical solution of muscle forces about the ankle joint with objective function of relative muscle forces, p=3

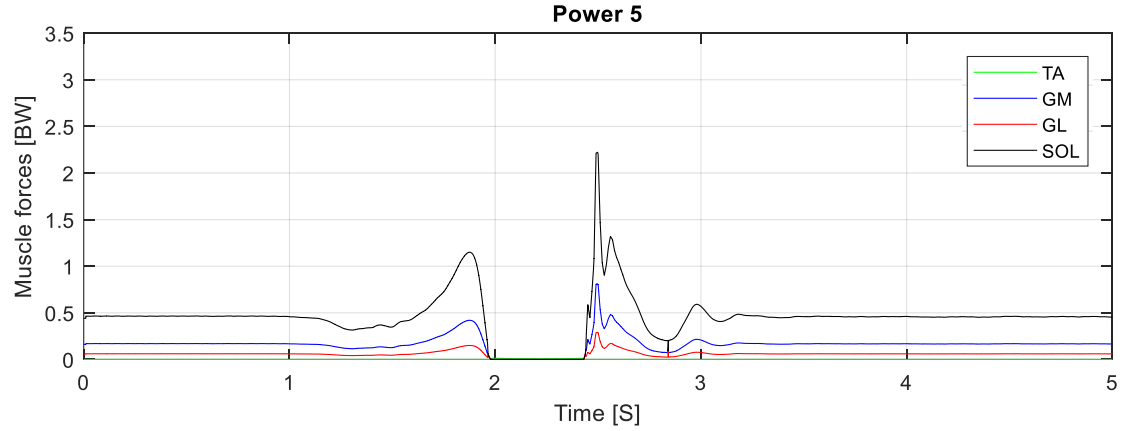

Figure 34: Numerical solution of muscle forces about the ankle joint with objective function of relative muscle forces, p=5

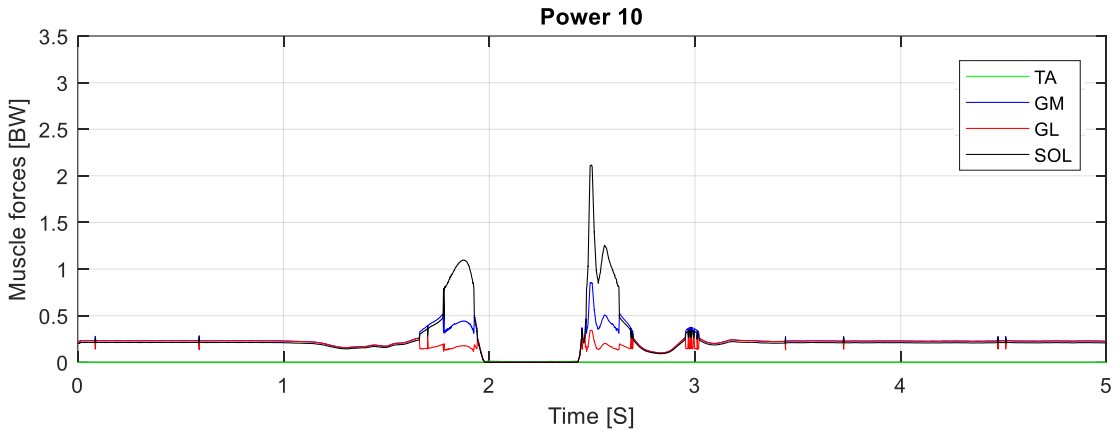

Figure 35: Numerical solution of muscle forces about the ankle joint with objective function of relative muscle forces, p=10

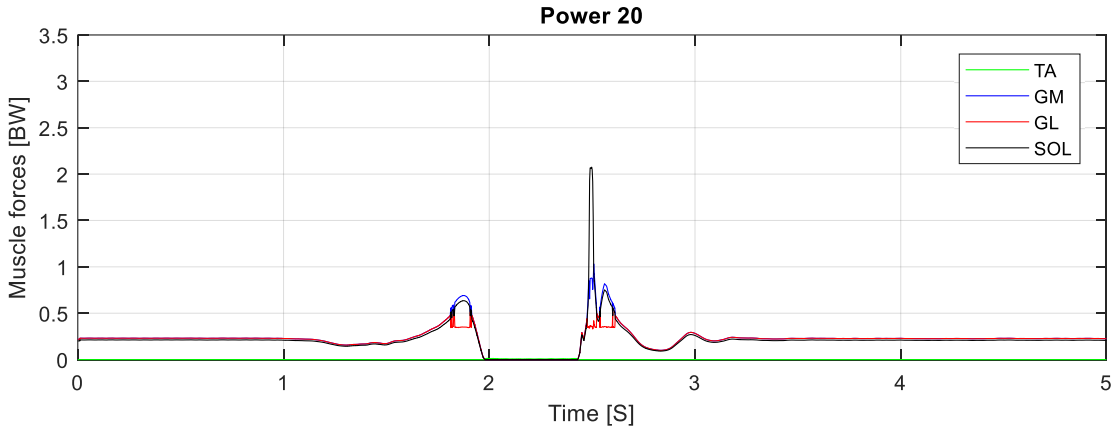

Figure 36: Numerical solution of muscle forces about the ankle joint with objective function of relative muscle forces, p=20

Table 4: Peak forces of muscles about the ankle joint during jumping and landing of CMJ - numerical approach with objective function of minimizing relative muscle forces to the power of 3, 10, and 20

Muscles Examined	**Peak Jumping Force (p=3)**	**Peak Landing Force (p=3)**	**Peak Jumping Force (p=10)**	**Peak Landing Force (p=10)**	**Peak Jumping Force (p=20)**	**Peak Landing Force (p=20)**
Soleus	1.240 BW	2.398 BW	1.094 BW	2.107 BW	0.687 BW	2.066 BW
Lateral Head of Gastrocnemius	0.051 BW	0.098 BW	0.106 BW	0.203 BW	0.117 BW	0.227 BW
Medial Head of Gastrocnemius	0.376 BW	0.727 BW	0.443 BW	0.855 BW	0.691 BW	0.949 BW

5.3 Analytical Approach

An analytical approach with Lagrangian multipliers was used to obtain muscle forces during a CMJ motion in a static optimization problem. In MATLAB, a code was generated to run this optimization. The analytical approach serves as a method of obtaining muscle forces in the form of a closed-form exact solution [49]. However, as the power of the criterion increases, the number of possible solutions increase significantly, and a unique solution does not exist. This method was shown to provide good results with a power of 2 or 3 for the criterion [50]. Thus, this approach was used to validate the numerical approach. To examine higher powers, a power of 10 was used under the same formulation to examine the results. To apply varying power of the criterion, a Lagrangian multiplier is incorporated for the non-linear optimization problem, to obtain the following expression for muscle forces [49]:

$$F_j = \tau_{joint} \cdot \left[r_j \cdot \sum_{i=1}^{n} \left\{ \frac{r_i \cdot a_i}{r_j \cdot a_j} \right\}^{\left(\frac{P}{P-1}\right)} \right]^{-1} \geq 0 \qquad (10)$$

where i≠j for a unique solution using Lagrangian multiplier, r_j is the moment arm of the j^{th} muscle, a_j is the physiological cross-sectional area of the j^{th} muscle, p is the power of the criterion and τ_{joint} is the total joint moment. To bound the problem, the equality and inequality constraints in equations 3-5 were used. This formulation leads to muscles of larger moment arms and physiological cross-sectional areas to be recruited first for muscle forces. For the analytical approach, the muscles about the ankle joint were of interest and were investigated with a power of 2, 3, and 10. Power of 3 was used to create a comparison between the analytical and numerical approaches of static optimization. A power of 10 was used to show the effect of high powers on the analytical approach.

The inputs of this problem are the joint moments and muscle moment arms from the musculoskeletal model, along with maximum isometric force and physiological cross-sectional area of all muscles recruited. The objective function of muscle stresses (equation 1) was the primary objective function of this approach. For the ankle joint, Figure 37 to Figure 39 show the result of static optimization under different powers of the objective function of relative muscle forces. In addition, Table 5 shows the peak forces of muscles during the jumping and landing phase of the countermovement jump.

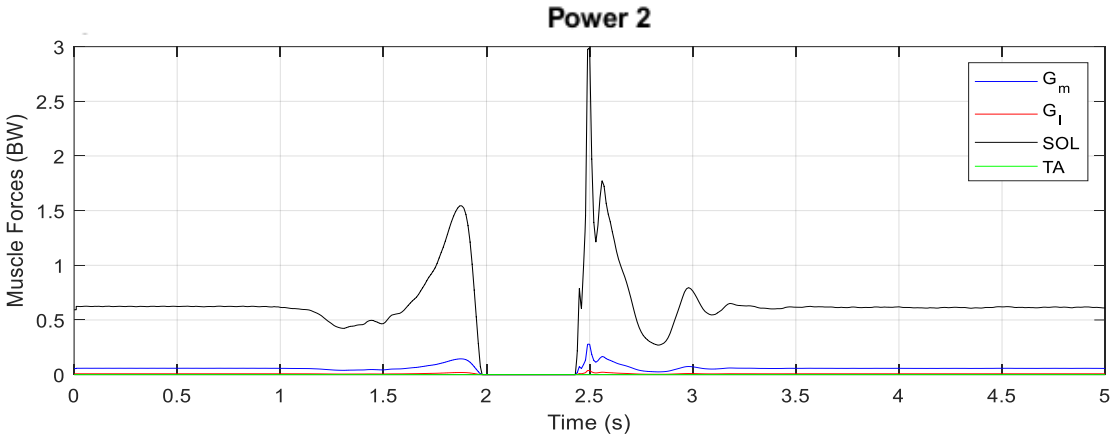

Figure 37: Analytical solution of muscle forces about the ankle joint with objective function of muscle stresses, p=2

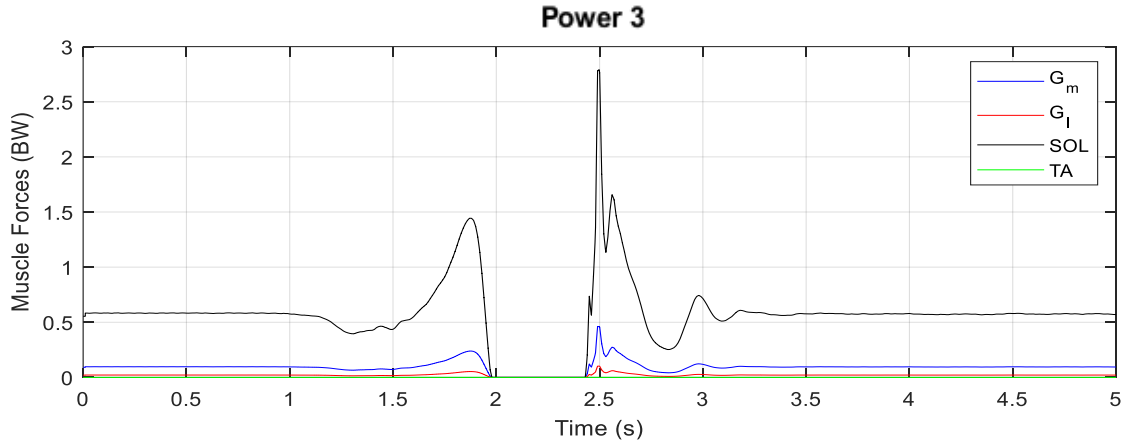

Figure 38: Analytical solution of muscle forces about the ankle joint with objective function of muscle stresses, p=3

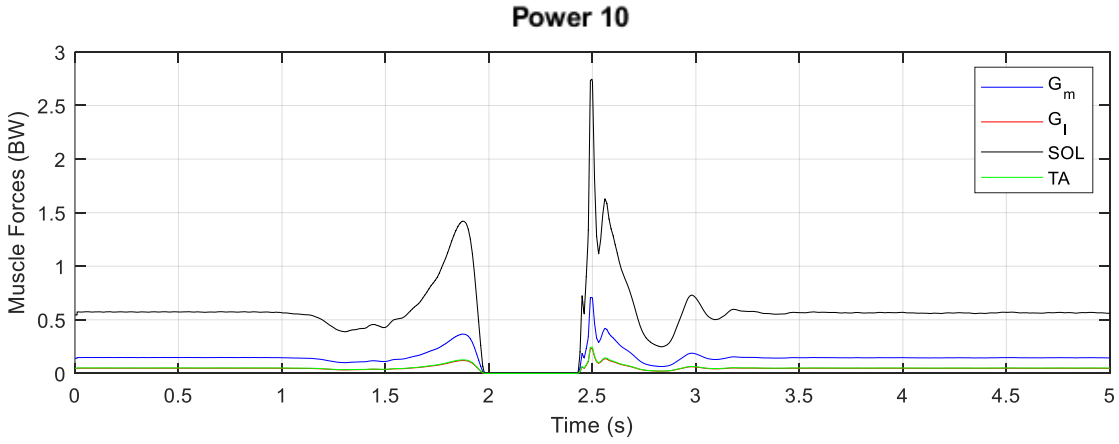

Figure 39: Analytical solution of muscle forces about the ankle joint with objective function of muscle stresses, p=10

Table 5: Peak forces of muscles about the ankle joint during jumping and landing of CMJ - analytical approach with objective function of minimizing muscle stresses to the power of 2, 3, and 10

Muscles Examined	**Peak Jumping Force (p=2)**	**Peak Landing Force (p=2)**	**Peak Jumping Force (p=3)**	**Peak Landing Force (p=3)**	**Peak Jumping Force (p=10)**	**Peak Landing Force (p=10)**
Soleus	1.544 BW	2.982 BW	1.443 BW	2.791 BW	1.419 BW	2.734 BW
Lateral Head of Gastrocnemius	0.019 BW	0.037 BW	0.053 BW	0.090 BW	0.123 BW	0.242 BW
Medial Head of Gastrocnemius	0.143 BW	0.278 BW	0.239 BW	0.460 BW	0.367 BW	0.706 BW

5.4Discussion

Overall, static optimization is a fast and simple pathway to tackle the problem of muscle redundancy. However, it does not fully capture the physiological nature of muscles. In this phase of the project, multiple investigations were conducted. This includes: (1) the use of numerical approach (fmincon function) of static optimization for muscle forces that actuate the hip, knee and, ankle joints, (2) the effect of varying the power of the objective function in the numerical approach of static optimization, (3) the effect of changing the objective function for the same motion in the numerical approach of static optimization, and (4) the use of analytical approach (Lagrangian multiplier) to conduct static optimization and its use for validating the numerical approach. The focus was mainly directed towards peak forces during the propulsion/jumping stage and the landing stage. These stages contributed to the highest forces during the motion and thus were analyzed in this section and used as inputs in the finite element modeling phase of this project.

For the **first analysis**, Table 1, Table 2, and Table 3 show the results of numerical static optimization obtained for muscle forces about the ankle, knee, and hip joints, respectively, during peak jumping and landing. These results are for the objective function of minimizing muscle stresses. Since a power of 3 for the criterion holds a physiological meaning of maximizing energy expenditure, it was used as the primary solution for this project [42]. To add to that, this project tackles the risk of injuries due to these forces. Thus, utilizing muscle forces with this power can give greater insight as it can give insight about energy expenditure and fatigue in muscles [43, 50]. Figures 16, 21 and 26 show the results of muscle forces using the objective function of minimizing muscle stresses with a power of 3 for the ankle, knee, and hip joint. For the motion studied, muscle forces were highest during peak jumping and landing for the soleus muscle, vasti muscle, and semimembranosus muscle. The soleus resulted in peak forces of 1.45 BW during jumping and 2.80 BW during landing. The vasti muscle resulted in peak forces of 2.35 BW during jumping and 4.05 BW during landing. To add to that, the semimembranosus muscle resulted in peak forces of 1.62 BW during jumping and landing. Other muscles also contributed high forces during the two force peaks of the motion. Overall, muscle forces were larger during the peak point of the landing stage than the propulsion phase for all the muscles examined in the static optimization problem.

Some muscles about the hip joint resulted in forces that reached their maximum isometric forces. This was not regarded as an issue in the results, as other muscles about the hip joint did not reach their maximum isometric force (Figure 26) and an impactful load of jumping and landing can impose high loads. The static optimization provided a solution to compute for the muscles investigated, taking into account their cross-sectional area and moment arms. In addition, injury of bone is of interest in this project and thus possible higher forces of muscles can provide better insight.

Previous research on peak muscle forces during vertical jumps showed similar ranges to results obtained in this thesis [49]. For example, vasti muscle resulted in a peak force of 3.27 BW during vertical jumps, reasonably comparable to the 3 BW obtained previously [49]. In addition, the bicep femoris muscle resulted in similar force values in this work (1.16 BW) and in previous research (1.1 BW) [49]. Overall, the muscle forces obtained in this work can be partially validated using previous research [49]. It must be noted that this previous research was conducted with the same objective function (muscle stresses) but at a power of 30. Thus, the values are comparable but not exact.

The **second analysis** investigated the effect of changing the power of the criterion in the numerical approach of static optimization. The powers used were 2, 3, 5, 10, and 20. Section 5.2 depicts all the different results obtained for the objective function of muscle stress under specified powers in figures 15 to 29. Through examining peak forces during jumping and landing stages in tables 1-3, consistent observation was present in all the results obtained. It is that by increasing the power of the criterion, better muscle synergy is observed. With a power of 2, one or two muscles seem to dominate the total force that actuate the joint. Larger powers lead to a better force distribution between muscles examined for each joint. For example, the soleus muscle has a peak force of 1.447 BW and the medial head of gastrocnemius has a peak force of 0.243 BW during jumping at a power of 3. With increasing the power to 10, the soleus muscle has a peak force of 1.279 BW and the medial head of gastrocnemius has a peak force of 0.334 BW during jumping. This observation was the same for all 3 joints analyzed in this static optimization problem. This analysis suggests that with increasing power of objective function, better synergy is observed between the muscle. Better synergy between muscles is desirable to avoid muscle fatigue and lower the risk of injury [45]. Higher powers of the objective function were also tested (p=30,

p=40), but the results did not vary in comparison to the power of 20 presented in this work. This suggests that the results tend to converge with increasing the power. The results of higher powers were utilized to examine the effect of having a better balance of forces applied to the tibia. However, a power of 3 was the focus of this work to examine the risk of injury of the tibial bone.

The **third analysis** investigated the effect of using a different objective function, minimizing relative muscle forces, in the numerical approach of static optimization. The same muscles and inputs were used; however, the physiological cross-sectional area was replaced with the maximum isometric forces of muscles. Table 6 below shows a comparison between the peak forces of jumping and landing of the two objective functions at powers of 3 and 10 to examine the difference. Overall, the pattern of results obtained was similar for lower powers, power of 2 or 3, between the two objective functions, as shown between figures 15-16 and figures 30-31. However, the difference in peak forces was respectively significant at the power of 3 and the power of 10. As the power increases for the objective function of relative muscle forces, larger muscle synergy was observed. However, at higher powers, the objective function of relative muscle forces does not provide smooth results for muscle forces as expected. A possible reason is that the inputs to the static optimization problem are inadequate in determining an optimal synergy between muscles at higher power of objective function. This can suggest that the objective function of relative muscle forces is inadequate for the motion studied, in comparison to the objective function of muscle stresses. Despite that, the objective function of relative muscle forces could be helpful for other motions, or it could be adequate for CMJ under a lower power of criterion. Nevertheless, this analysis directed the focus of the static optimization problem toward the use of the objective function of muscle stresses.

Table 6: Comparison of peak forces of muscles about the ankle joint during jumping of CMJ - numerical approach with objective functions of muscle stresses and relative muscle forces

Muscles Examined	**Peak Jumping Force (p=3)** Muscle stress	**Peak Jumping Force (p=3)** Relative muscle force	**% Difference**	**Peak Jumping Force (p=10)** Muscle stress	**Peak Jumping Force (p=10)** Relative muscle force	**% Difference**
Soleus	1.447 BW	1.240 BW	14	1.279 BW	1.094 BW	14
Lateral Head of Gastrocnemius	0.051 BW	0.051 BW	0	0.106 BW	0.106 BW	0
Medial Head of Gastrocnemius	0.243 BW	0.376 BW	35	0.334 BW	0.443 BW	24

The **fourth and final analysis** investigated the analytical approach of static optimization to obtain muscle forces during a CMJ. This method was explored as a closed-form solution and a mathematical alternative to using the fmincon function in the numerical approach. Moreover, this method can be used as a method of validating the muscle forces obtained during the numerical approach with lower power of criterion (power of 2 or 3) [50]. Table 7 below shows a comparison between the numerical and analytical approaches of static optimization with the objective function of muscle stresses and power of 3. The percentage difference in muscle forces obtained ranges between 0% to 4%. This is considered to be relatively small and thus validates the results obtained from the numerical approach of static optimization.

The analytical approach was also investigated using the objective function with a power of 10. For a power of 2 or 3, the analytical approach can obtain good results through the use of Lagrangian multipliers. However, as the power increases, the optimization constraints are no longer met, and the results of muscle forces are greatly affected [50]. As shown in figure 39, tibialis anterior muscle was activated during the peak forces of jumping and landing, where extension of

the ankle takes place, despite it being a flexor muscle. In addition, the results obtained for a power of 10 in the analytical approach are significantly different in comparison to the results obtained for a power of 10 in the numerical approach. This supports the limitation of using the analytical approach at higher powers of criterion [50]. Thus, the analytical approach should only be used with power of 2 or 3 to provide a closed-form solution to the problem of static optimization.

Table 7: Comparison of peak forces of muscles about the ankle joint during jumping of CMJ - numerical approach and analytical with objective function of muscle stresses

Muscles Examined	**Peak Jumping Force (p=3)** Numerical	**Peak Jumping Force (p=3)** Analytical	**% Difference**
Soleus	1.447 BW	1.443 BW	0.28%
Lateral Head of Gastrocnemius	0.051 BW	0.053 BW	3.77%
Medial Head of Gastrocnemius	0.243 BW	0.239 BW	1.67%

Chapter 6

6 Finite Element Model of the Tibia

This chapter covers phase VI of the project, tackling the objective of obtaining tibial stresses, strains, and deformations during countermovement jumping. This chapter utilizes several components at different phases of this work to obtain realistic and meaningful finite element analysis of the tibia. For the finite element analysis, 3 simulations were conducted. This includes a standing state simulation, a peak jumping/propulsion simulation, and a peak landing simulation.

6.1 Material Properties and Constitutive Laws

To conduct the finite element (FE) analysis, a tibia model was obtained and adapted from previous research [51]. The model was obtained from a subject's CT scan of the left leg, and the images were analyzed to form a bone model. The model was meshed with quadratic tetrahedral elements to approximately 220,000 elements. A convergence test was conducted to ensure that the meshing is adequate for the motion studied. The FE analysis was conducted in ABAQUS 2017 (Abaqus inc., USA).

Bone was modeled as an inhomogeneous isotropic material. This was done by correlating an elastic constant of one direction to the apparent bone density obtained from imaging. This elastic modulus was then used to obtain other elastic properties, similar to previous literature [51-52]. Figure 40 shows an illustration of the meshed model of the tibia.

Figure 40: Meshed model of the human tibia

6.2 Loading and Boundary Conditions

Two different loading and boundary conditions were utilized for analysis. The first set of conditions and constraints were based off previous literature [51, 53].

For the first scenario, the boundary condition was a pinned constraint at the distal tibia, at the midpoint of the left and right malleoli, to only allow rotation about the ankle center. In addition, a point on the tibial plateau (proximal end) was fixed in the anterior-posterior and medial-lateral directions for the application of knee joint contact forces. This point is located at the center of pressure of the tibia [54]. For this scenario, the loading condition of this model included the knee joint contact force and the muscle forces obtained in phase V of this project. Muscle points of insertions and line of actions were used and scaled for this model [39, 40]. It must be noted that the subject of the CMJ data collection is not the same subject of the tibia model. Thus, minor scaling (×1.05) took place to match the parameters, such as the points of insertion of muscles. Each muscle force was applied to approximately the nearest node on the tibia model. All the muscles incorporated in the static optimization problem were added to this model. All forces were added as concentrated forces. Overall, the analysis was conducted for a standing stage, peak forces during the propulsion stage, and peak forces during the landing stage.

For the second scenario, more realistic loading and boundary conditions were desired. The tibia bone is expected to be loaded at both the proximal and distal ends of the tibia. Thus, the ankle joint contact forces were added to the model at the distal end at the midpoint of the left and right malleoli. Otherwise, all other parameters and conditions were kept unchanged, in comparison to the first scenario. An illustration of the loads applied in scenario 2 is depicted in Figure 41.

The finite element analysis was composed of investigating stresses, strains and deformation of the tibia during standing, propulsion, and landing. This was to provide insight over the mechanical behavior of bone under loading of CMJ. With muscle contractions, impact loading, and gravitational force, the bone experiences applied stress (load per unit area) [55]. This stress leads to strain in the bone, which is deformation of the bone relative to original dimensions [55]. In locations of smaller cross-sectional area, localized stresses/strains are expected to be higher [55]. This analysis of the tibia provides insight about localized higher stresses-strains and maximum stress/strain. Magnitude of deformation provides a metric measurement of strain.

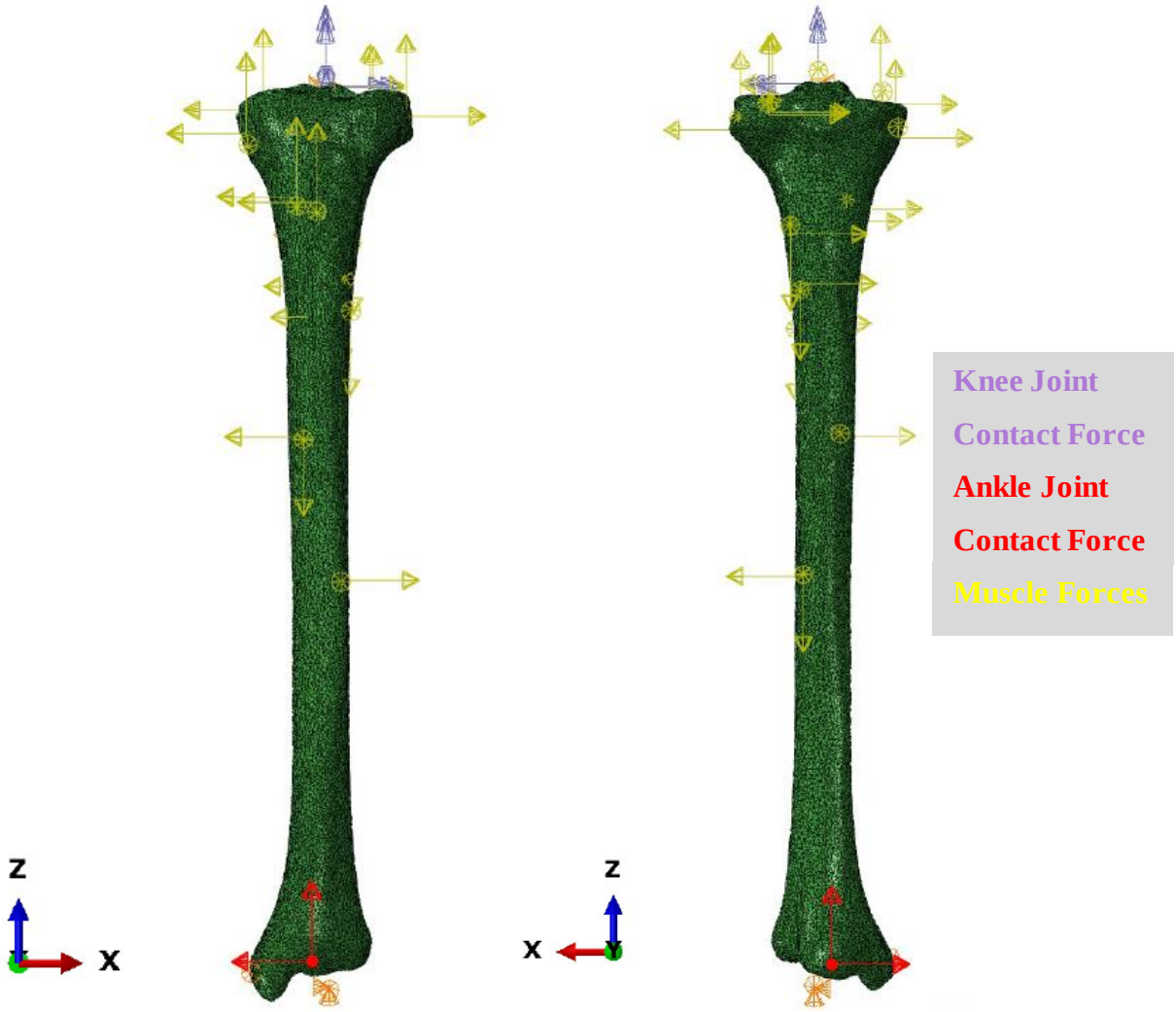

Figure 41: Illustration of the loads applied to the model, including muscle forces (yellow vectors), knee joint contact forces (purple vectors), and ankle joint contact force (red vectors) - Scenario 2

6.3 FEM Results of Standing State

For the standing state, joint contact forces were obtained from the dynamics simulation and muscle forces were obtained from the static optimization results. Scenario 1 only included knee joint contact forces, while the distal end is pinned. Figure 42 shows the results for the maximum principal strain in the tibia model. Figure 43 shows the results for the maximum principal stress in the tibia model. Figure 44 shows the results for the magnitude of translation deformation in the tibia model.

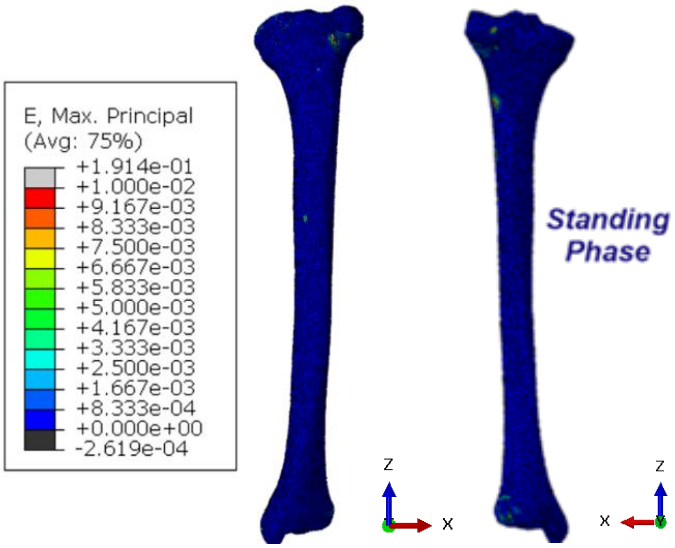

Figure 42: Maximum principal strain of the tibia under knee joint contact force (scenario 1) – Standing

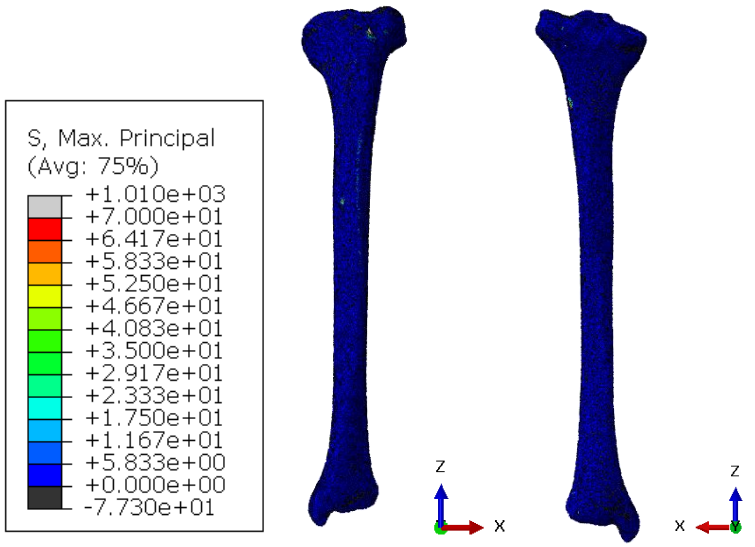

Figure 43: Maximum principal stress of the tibia under knee joint contact force (scenario 1) – Standing

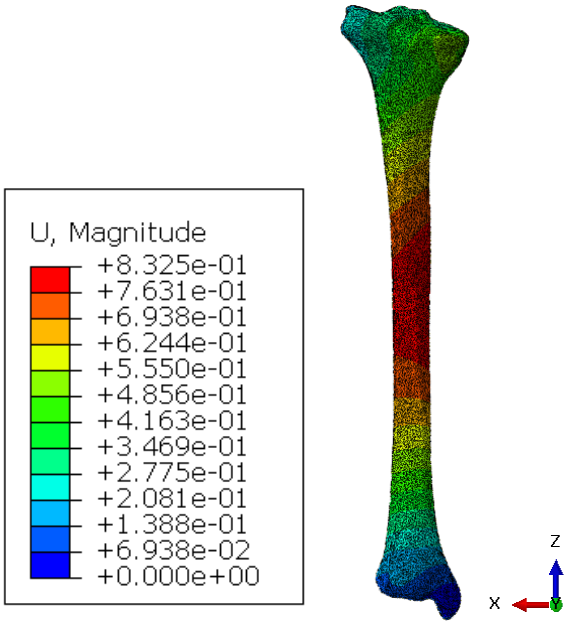

Figure 44: Magnitude of translational of the tibia under knee joint contact force (scenario 1) – Standing

Scenario 2 included knee and ankle joint contact forces to the model. Figure 45 shows the results for the maximum principal strain in the tibia model. Figure 46 shows the results for the maximum principal stress in the tibia model. Figure 47 shows the results for the magnitude of translation deformation in the tibia model.

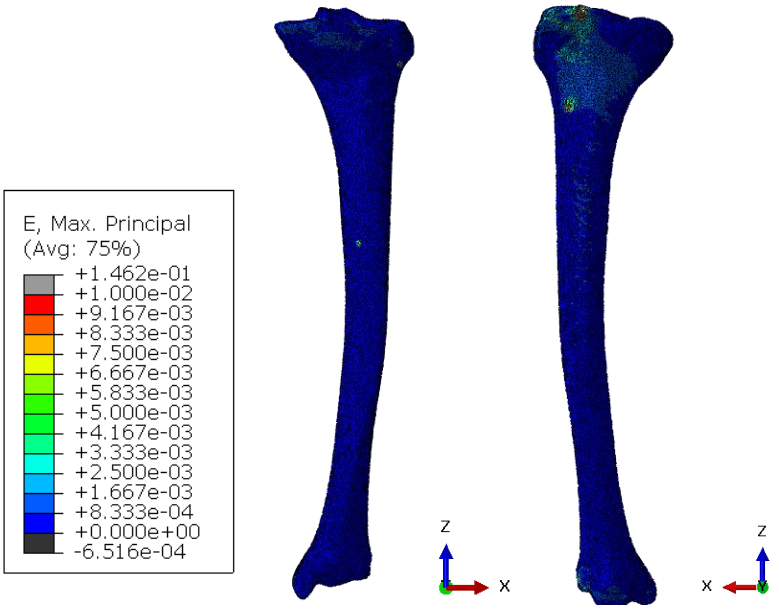

Figure 45: Maximum principal strain of the tibia under knee and ankle joint contact forces (scenario 2) – Standing

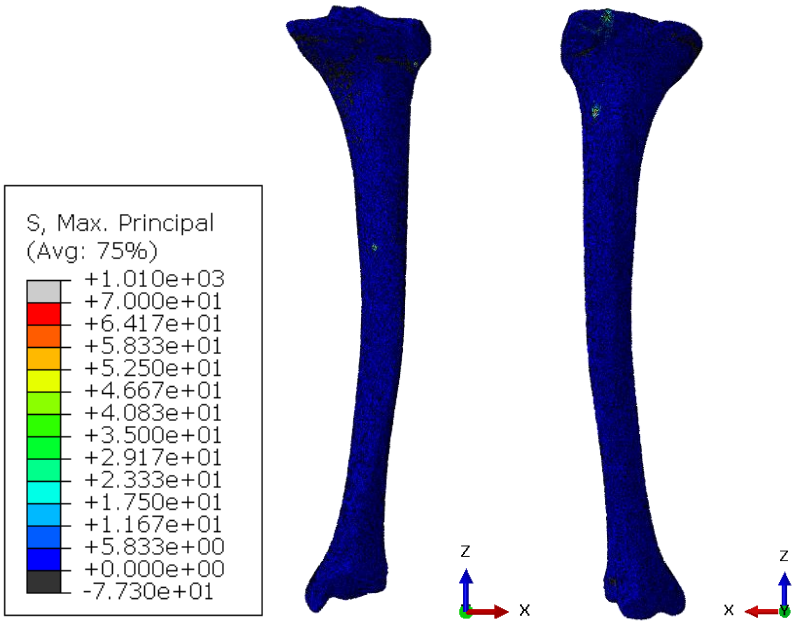

Figure 46: Maximum principal stress of the tibia under knee and ankle joint contact forces (scenario 2) – Standing

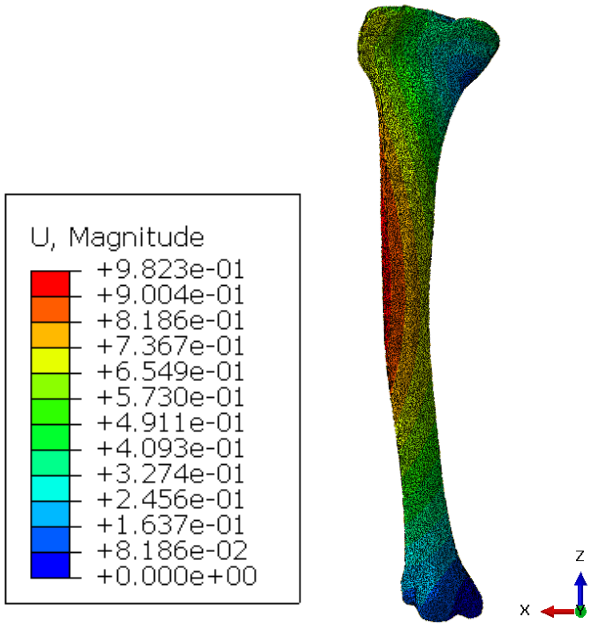

Figure 47: Magnitude of translational deformation of the tibia under knee and ankle joint contact forces (scenario 2) – Standing

6.4FEM Results of CMJ Jumping

For the jumping/propulsion phase, joint contact forces were obtained from the dynamics simulation and muscle forces were obtained from the static optimization results (similar to the standing state). Scenario 1 only included knee joint contact forces, while the distal end was pinned. Figure 48 shows the results for the maximum principal strain in the tibia model. Figure 49 shows the results for the maximum principal stress in the tibia model. Figure 50 shows the results for the magnitude of translation deformation in the tibia model.

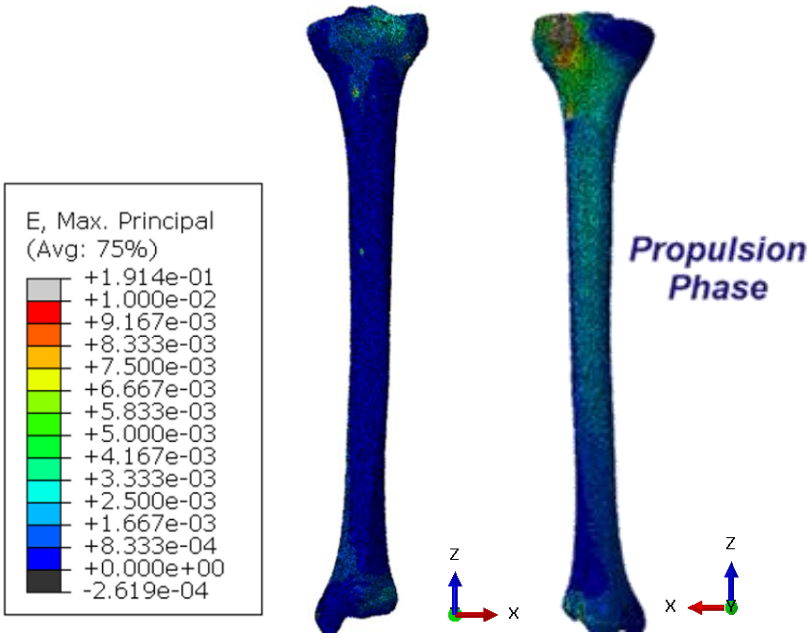

Figure 48: Maximum principal strain of the tibia under knee joint contact force (scenario 1) – Jumping

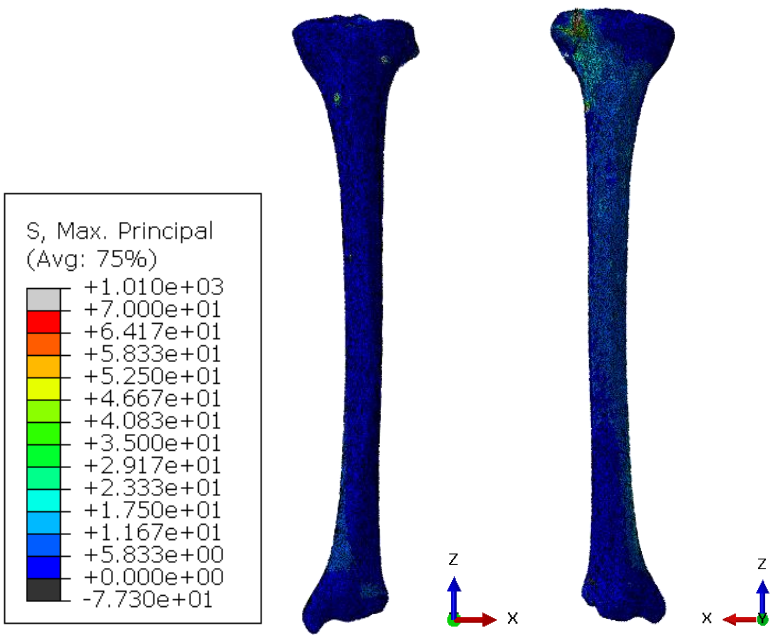

Figure 49: Maximum principal stress of the tibia under knee joint contact force (scenario 1) – Jumping

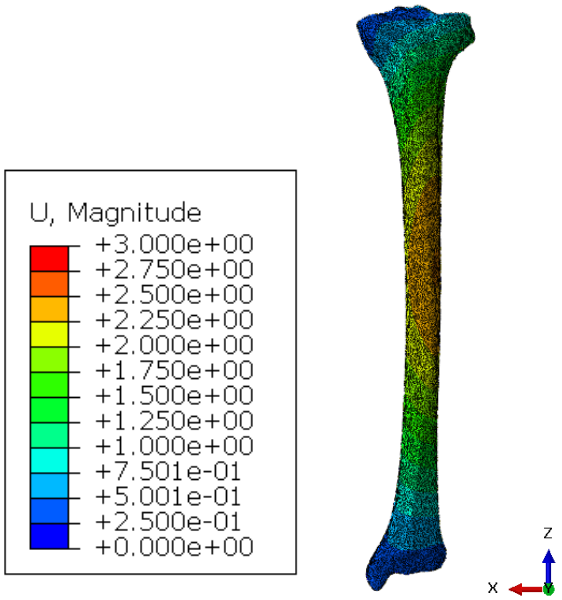

Figure 50: Magnitude of translation deformation of the tibia under knee joint contact force (scenario 1) – Jumping

Scenario 2 included knee and ankle joint contact forces to the model. Figure 51 shows the results for the maximum principal strain in the tibia model. Figure 52 shows the results for the maximum principal stress in the tibia model. Figure 53 shows the results for the magnitude of translation deformation in the tibia model.

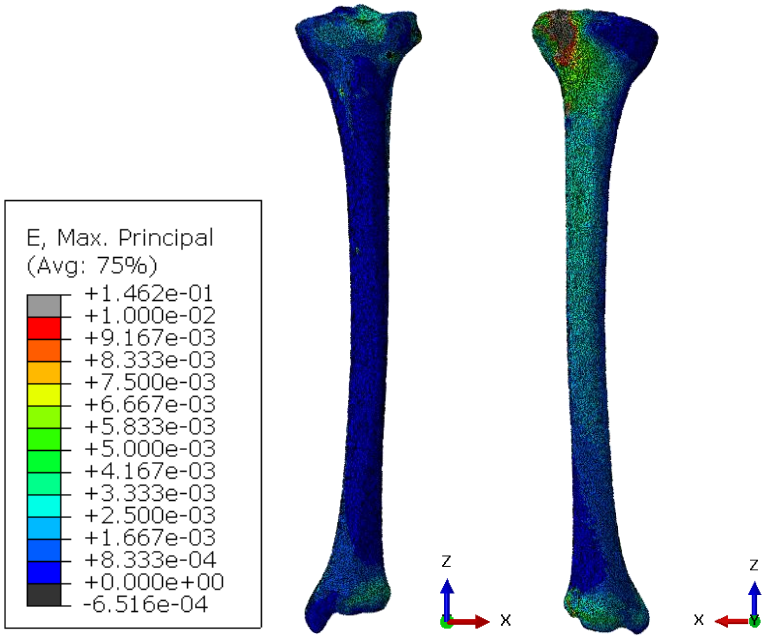

Figure 51: Maximum principal strain of the tibia under knee and ankle joint contact forces (scenario 2) – Jumping

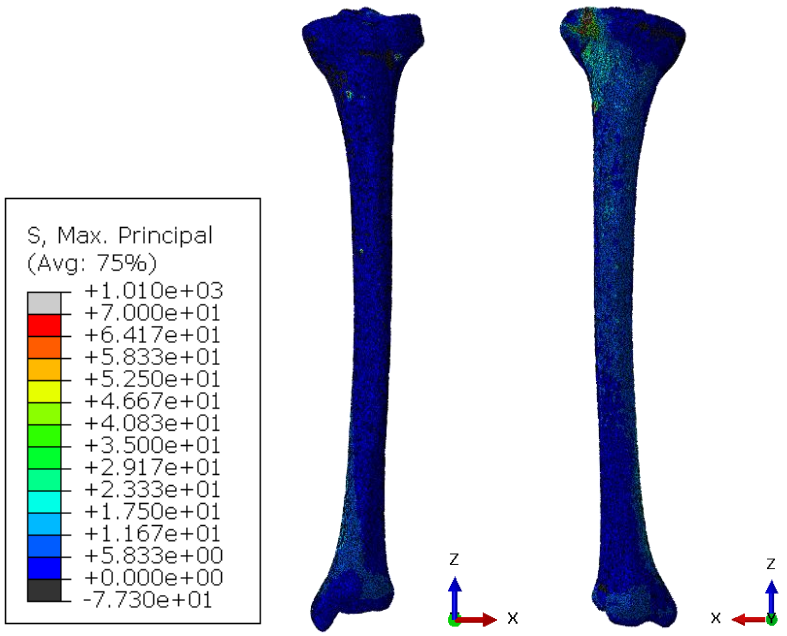

Figure 52: Maximum principal stress of the tibia under knee and ankle joint contact forces (scenario 2) – Jumping

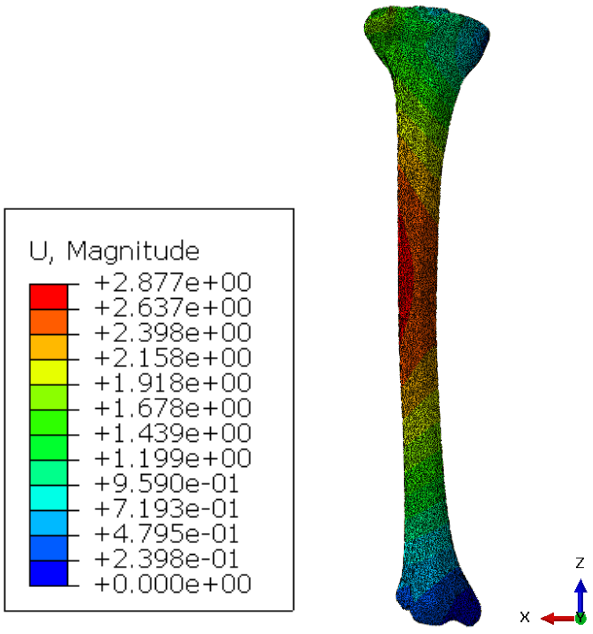

Figure 53: Magnitude of translational magnitude of the tibia under knee and ankle joint contact forces (scenario 2) – Jumping

In addition, results of the directional translational deformation of scenario 2 for the jumping state was obtained, as shown in Figure 54 to Figure 56.

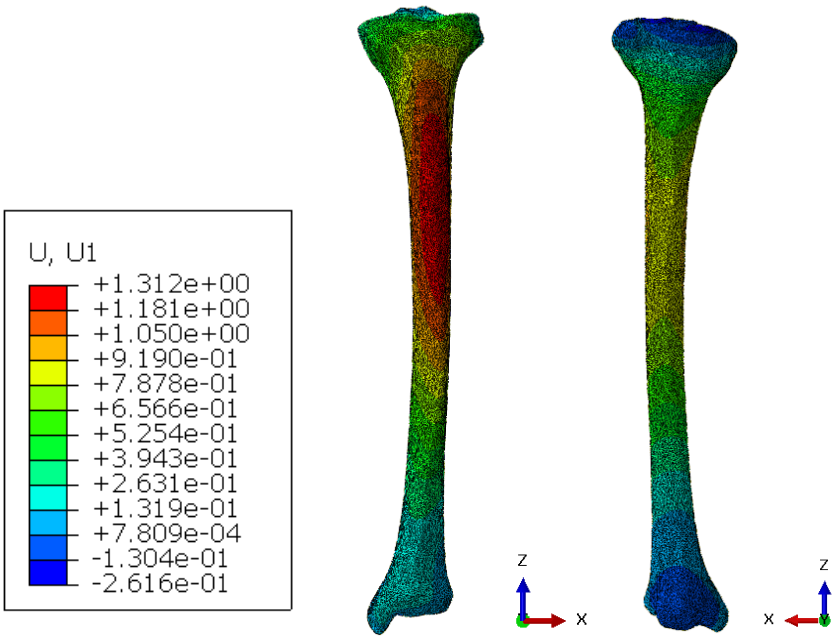

Figure 54: Horizontal translational magnitude of the tibia under knee and ankle joint contact forces (scenario 2) – Jumping

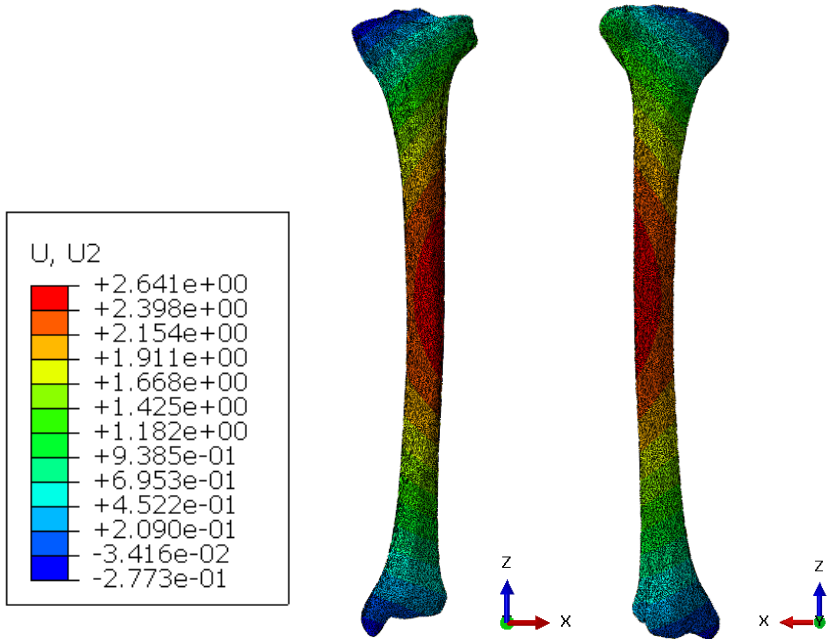

Figure 55: Vertical translational magnitude of the tibia under knee and ankle joint contact forces (scenario 2) – Jumping

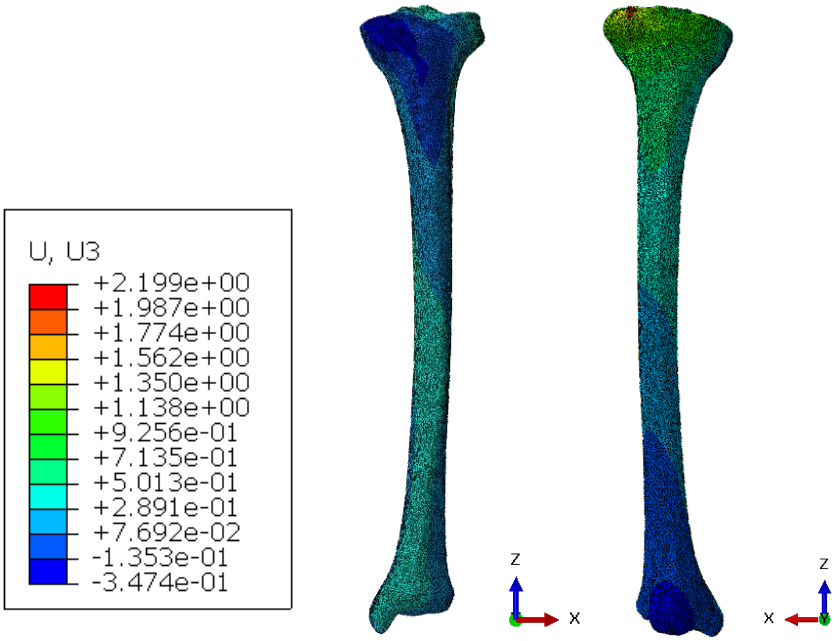

Figure 56: Axial translational magnitude of the tibia under knee and ankle joint contact forces (scenario 2) – Jumping

6.5 FEM Results of CMJ Landing

For the jumping/propulsion phase, joint contact forces were obtained from the dynamics simulation and muscle forces were obtained from the static optimization results (similar to the standing state). Scenario 1 only included knee joint contact forces, while the distal end is pinned. Figure 57 shows the results for the maximum principal strain in the tibia model. Figure 58 shows the results for the maximum principal stress in the tibia model. Figure 59 shows the results for the magnitude of translation deformation in the tibia model.

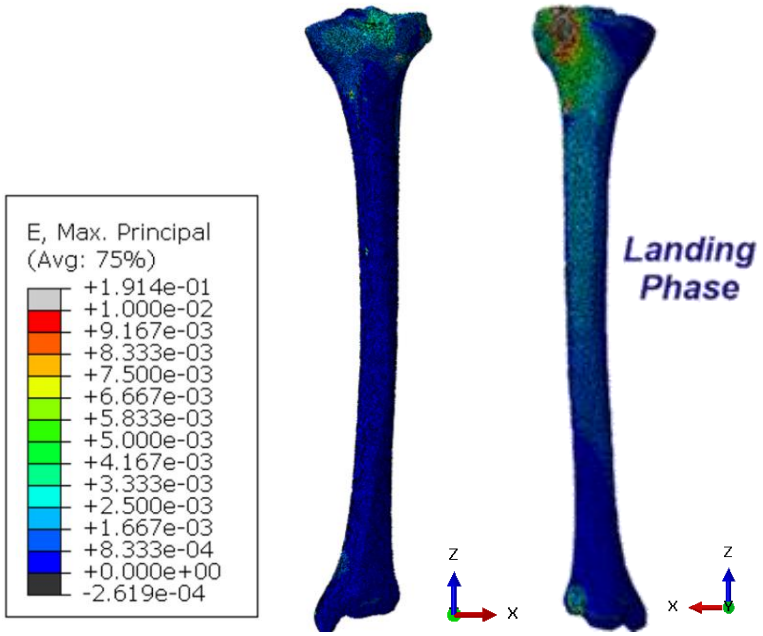

Figure 57: Maximum principal strain of the tibia under knee joint contact force (scenario 1) – Landing

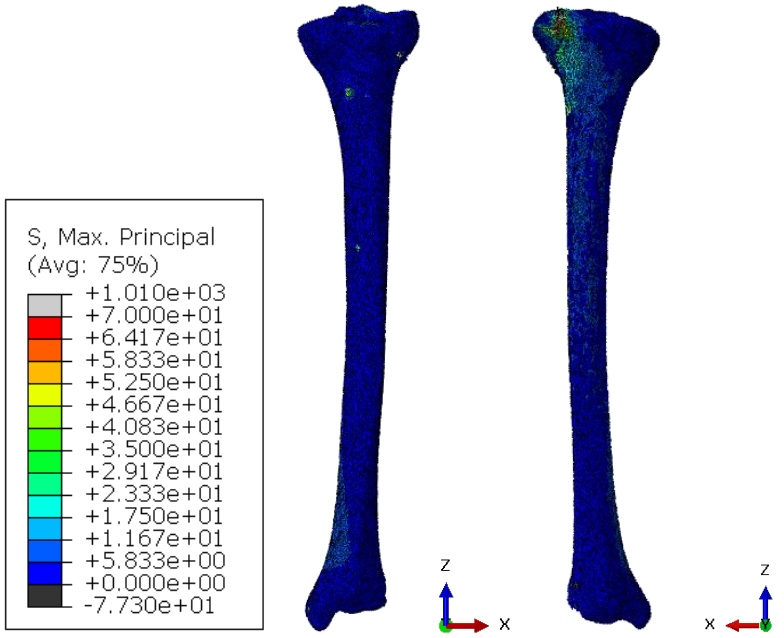

Figure 58: Maximum principal stress of the tibia under knee joint contact force (scenario 1) – Landing

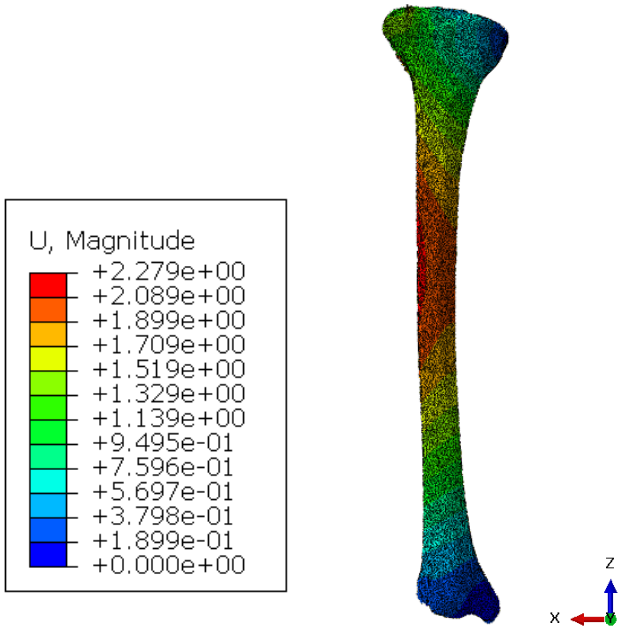

Figure 59: Magnitude of translational deformation of the tibia under knee joint contact force (scenario 1) – Landing

Scenario 2 included knee and ankle joint contact forces to the model. Figure 60 shows the results for the maximum principal strain in the tibia model. Figure 61 shows the results for the maximum principal stress in the tibia model. Figure 62 shows the results for the magnitude of translation deformation in the tibia model.

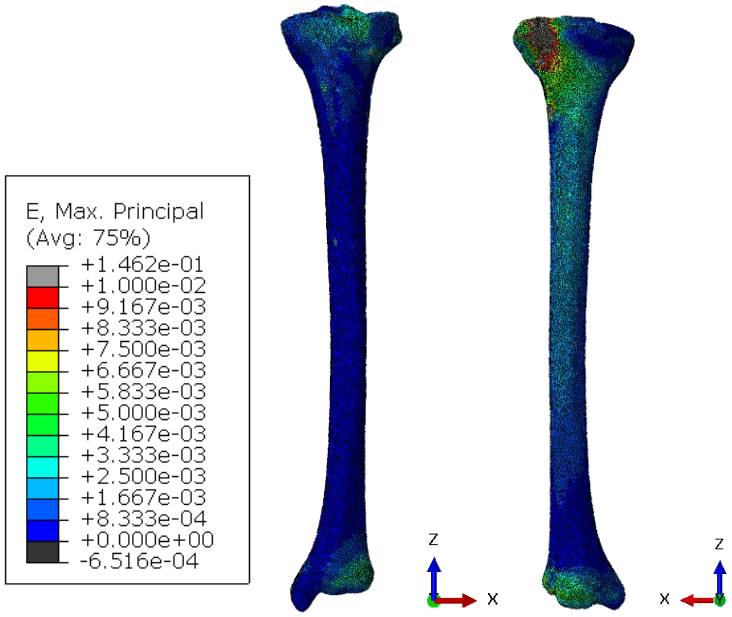

Figure 60: Maximum principal strain of the tibia under knee and ankle joint contact forces (scenario 2) – Landing

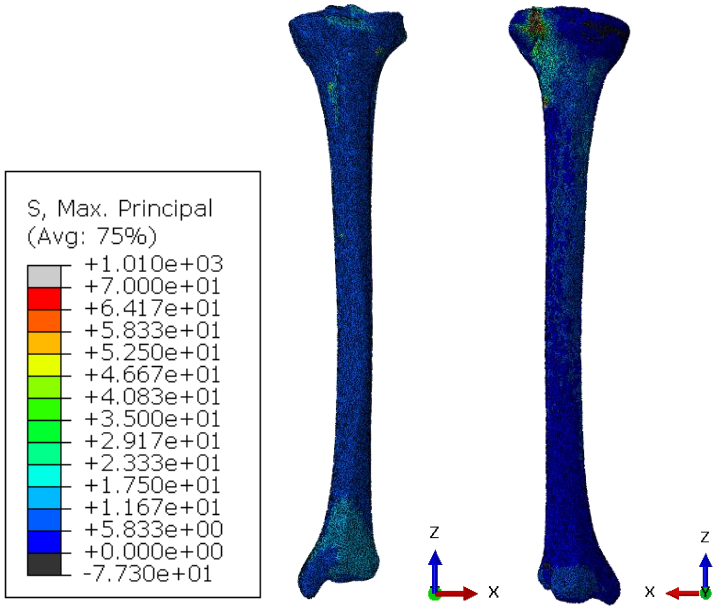

Figure 61: Maximum principal stress of the tibia under knee and ankle joint contact forces (scenario 2) – Landing

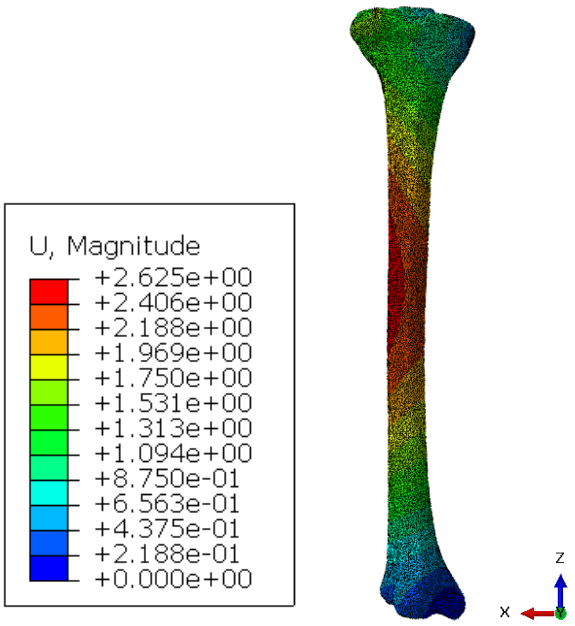

Figure 62: Magnitude of translational magnitude of the tibia under knee and ankle joint contact forces (scenario 2) – Landing

In addition, results of the directional translational deformation of scenario 2 for the jumping state was obtained, as shown in Figure 63 to Figure 65.

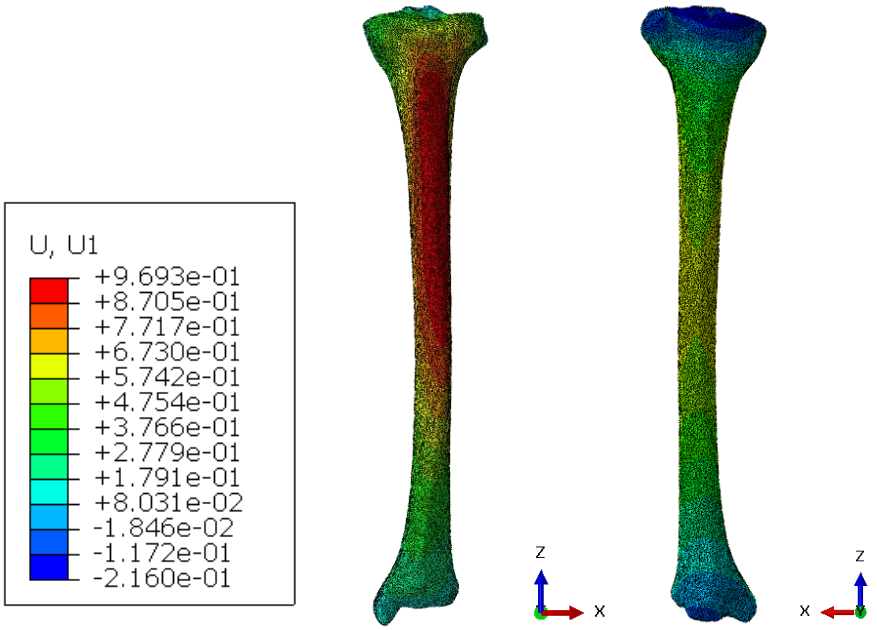

Figure 63: Horizontal translational magnitude of the tibia under knee and ankle joint contact forces (scenario 2) – Landing

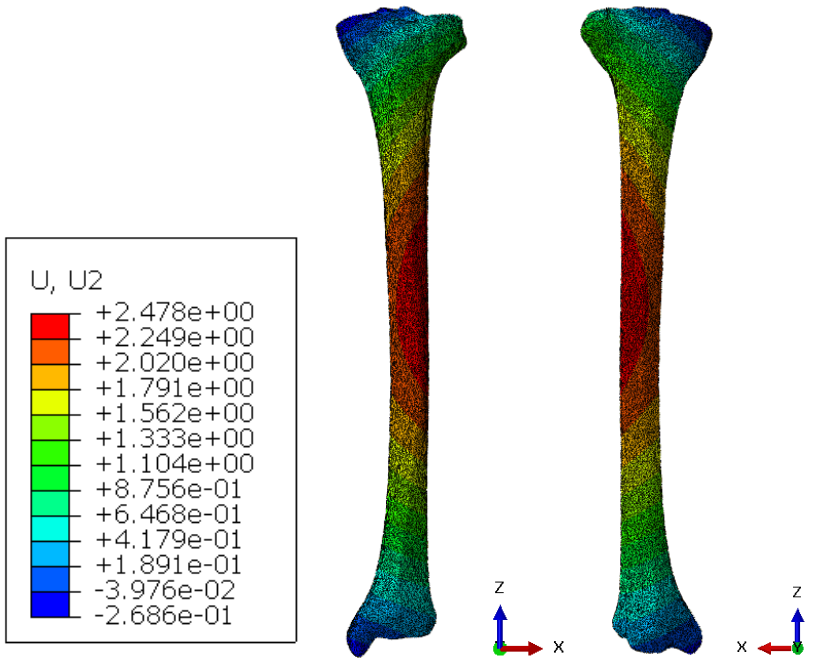

Figure 64: Vertical translational magnitude of the tibia under knee and ankle joint contact forces (scenario 2) – Landing

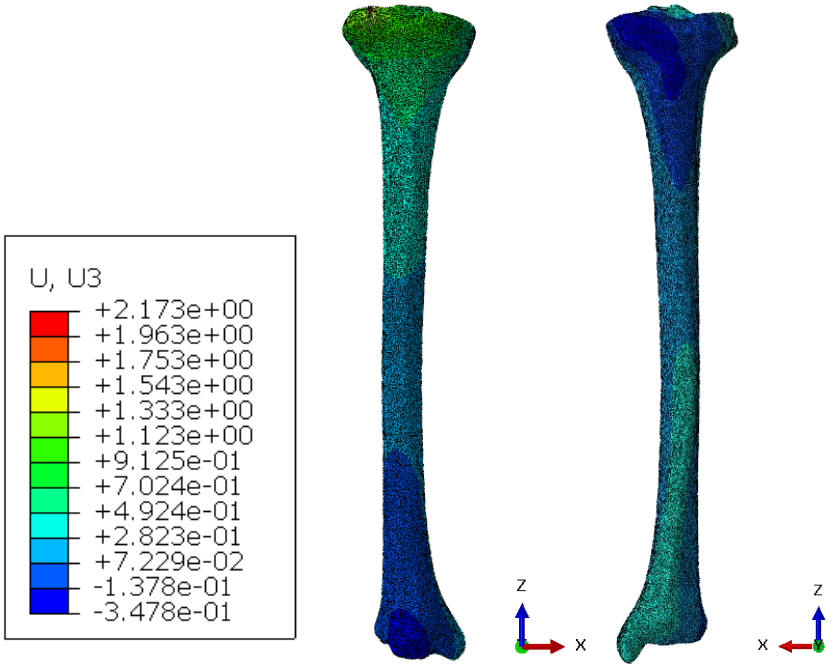

Figure 65: Axial translational magnitude of the tibia under knee and ankle joint contact forces (scenario 2) – Landing

6.6 Discussion of FEM Results

Finite element modeling is a numerical approximation method to analyze the structural behavior of complex components. It utilizes partial differential equations for the structural description of the continua [56]. This computational method breaks down a geometric model into a finite number of elements and performs many numerical operations for every element in the model [56]. A graphical representation of the full model is the output of this simulation, where a continuum result is obtained [56]. In this work, a stress analysis was conducted on the complex geometry of the tibia. With impact loads are exerted on the bone during CMJ, mechanical stress is applied. This causes a localized strain at a certain location on the bone, which leads to deformation of the bone that can be either temporary or permanent. For this project, the medial shaft of the tibia is of greater interest as a tool to understand stress fractures and risk of injuries (due to higher stress concentration).

Various results are presented in sections 6.3 to 6.5. Finite element analysis of the tibia during CMJ includes: (1) Analysis of stress, strain, and magnitude of translational deformation of the tibial bone during standing, (2) Analysis of stress, strain, and magnitude of translational deformation of the tibial bone during jumping, (3) Analysis of orthogonal translational deformations of the tibial bone during jumping, (4) Analysis of stress, strain and magnitude of translational deformation of the tibial bone during landing, and (5) Analysis of orthogonal translational deformations of the tibial bone during landing. In addition, this section covers a comparison between jumping and landing, along with highlighting the significance of these results to stress fractures. Each analysis was performed under two scenarios, scenario 1 of pinning the distal end of the tibia and loading the proximal end with knee joint contact force, and scenario 2 of loading the proximal end and the distal end of the tibia with knee and ankle joint contact forces, respectively. Overall, results for strain values were compared to previous literature, particularly compared to in-vivo measurements of strain in the tibial shaft. To add to that, stress results were incorporated to investigate regions with risk of injuries, along with examining the deformation that takes place in the bone. Note that the tibia is modeled as a cortical bone, and its yield properties include tensile yield stress of 71 MPa and compressive yield stress of 135 MPa [57].

Section 6.3 includes the results obtained for a quasi-static analysis of the tibia under loading conditions of the standing phase of a countermovement jump. For scenario 1, the maximum principal strain was approximately +360 µstrains (min: +225 µstrains and max: +495 µstrains) along the tibial shaft. For scenario 2, the maximum principal strain was approximately +360 µstrains (min: +273 µstrains and max: +584 µstrains) along the tibial shaft. Various in-vivo measurements reported values of strain that range from +381 to +646 µstrains [58]. Overall, the strain values fall in the range of in-vivo strain values reported in literature.

For scenario 1, the maximum principal stress was averaging at approximately 5.92 MPa along the tibial shaft. For scenario 2, the maximum principal stress was averaging at approximately 6.03 MPa along the tibial shaft. No localized stress concentration was present in both simulations of the standing phase. In addition, the stresses obtained during this stage are very low in comparison to the yield stress of cortical bone. Moreover, very small translational deformation (max: 0.8 mm) was observed for the standing phase, with the highest deformation at the mid-shaft of the tibia.

Section 6.4 includes the results obtained for a quasi-static analysis of the tibia under loading conditions of the jumping/propulsion phase of a countermovement jump. For scenario 1, the maximum principal strain was approximately +1745 µstrains (max: +2656 µstrains) along the tibial shaft. For scenario 2, the maximum principal strain was approximately +2056 µstrains (min: max: +2939 µstrains) along the tibial shaft. Overall, a higher localized strain was observed along the anterior crust of the tibial shaft. For in-vivo measurements, values reported in the literature of strain range from +1858 to +2180 µstrains in the midshaft during vertical jumps [58]. Overall, the strain values fall in the range of in-vivo strain values reported in literature. However, the strain values in the localized region of the anterior crust of the tibial shaft were higher than the values obtained experimentally. This is possibly due to higher jumping associated with the CMJ motion studied (28 cm), in comparison to previous literature (10-15 cm) [58].

For scenario 1, the maximum principal stress was averaging at approximately 16.4 MPa (max: 24.3 MPa) along the tibial shaft. For scenario 2, the maximum principal stress was averaging at approximately 17.2 MPa (max: 26.2 MPa) along the tibial shaft. The stresses obtained during this stage are significantly higher under loads of the jumping phase. Previous research showed that fractures can take place in the cortical bone of a male at maximum principal stress of 42.77 MPa

[59]. This suggests that under repetitive high loads of jumping, the possibility of an injury or a stress fracture in the bone is higher at stresses lower than the yield stress. To add to that, this amplifies the need of analyzing the bone with a longer duration of stress exposures (i.e. fatigue) in the future, to closely examine the possibility of stress fractures in the tibial shaft. Significant translational deformation (max: 2.37 mm in scenario 1 and max: 2.88 mm in scenario 2) was observed for the jumping phase, with the highest deformation at the mid-shaft of the tibia. Most of the translational deformation took place in the vertical direction (along the axis of the bone), as shown in Figure 55.

Section 6.5 includes the results obtained for a quasi-static analysis of the tibial bone under loading conditions of the landing phase of a countermovement jump. For scenario 1, the maximum principal strain was approximately +1666 µstrains (max: +2512 µstrains) along the tibial shaft. For scenario 2, the maximum principal strain was approximately +2017 µstrains (max: +2885 µstrains) along the tibial shaft. Overall, a higher localized strain was observed along the anterior crust of the tibial shaft. For in-vivo measurements, reported values in the literature of strain range from +1420 to +2300 µstrains in the midshaft during drop landing [58]. Similarly, the strain values are in good correlation to in-vivo strain values. However, the strain values in the localized region of the anterior crust of the tibial shaft were higher than the values obtained experimentally. This was also observed in jumping simulation and is possibly due to the different landing techniques conducted in this study and the height to land.

For scenario 1, the maximum principal stress was averaging at approximately 16.2 MPa (max: 24.0 MPa) along the tibial shaft. For scenario 2, the maximum principal stress was averaging at approximately 16.9 MPa (max: 26.2 MPa) along the tibial shaft. The stresses obtained during this stage are significantly higher under loads of the landing phase. Significant translational deformation (max: 2.28 mm in scenario 1 and max: 2.63 mm in scenario 2) was observed for the landing phase, with the highest deformation at the mid-shaft of the tibia. Most of the translational deformation took place in the vertical direction (along the axis of the bone), as shown in Figure 64.

Overall, the stress distribution under loads of the landing phase is very similar to that of the jumping phase. However, the jumping phase resulted in slightly higher stress and strain values surrounding the anterior crust of the tibial shaft. This was unexpected as the loads of the landing phase are larger than the loads of the jumping phase. A possible reason for this observation could be due to the muscles recruited in this model. The same muscles were recruited for both the jumping and landing phase, and the line of action of each muscle determines the direction of the force application. Under these conditions, the bone can experience some loads that can counteract other loads, and thus lead to the results obtained (i.e. muscle extensors and flexors, magnitude of joint contact forces). With lower cross-sectional area along the anterior crust, higher stress, strain and deformation was expected and justifiable. To provide another source of comparison to the finite element model of this work, Von Mises stresses were examined during peak jumping and landing points of the countermovement jump. Along the tibial shaft, peak Von Mises stress during jumping was 41.027 MPa and peak Von Mises stress during landing was 41.9151 MPa. Based on the knowledge of the author, no finite element model exists for the tibia during jumping/landing motions. Thus, this model was compared to the finite element model of the tibia during walking [4]. In this work, peak Von Mises stress during walking was predicted to be 24.1 MPa [4]. Future work that tackles stresses and strain of the tibia is essential to fully validate the stresses obtained in this model.

The finite element analysis provided an investigation of the bone response under high impact loads that lead to injuries, such as stress fractures. The stresses in the bone were significantly higher during jumping and landing, in comparison to the results obtained in the standing phase, as expected. Repetitive jumping and landing that take place in many sports can impose repetitive impact loads on the bone [12]. This can lead to significant microdamage in the bone and ultimately lead to a stress fracture [12, 27].

Chapter 7

7 Conclusions

This thesis provided a framework for utilizing a musculoskeletal biomechanical model and a finite element model to investigate the motion of countermovement jumps. The presented work allows analyzing the dynamics of the body and the stress response of the bone (tibia) under the impact loading of jumping and landing. The results presented in this thesis signifies as an advanced tool in the training of athletes and in providing greater insight into bone response under meaningful loading conditions.

7.1 Thesis Summary

The purpose of this thesis was to utilize musculoskeletal multibody modeling and finite element modeling to examine impact dynamics and stresses/strains in the human tibia, respectively, of a countermovement jump. In completing this work: Chapter 2 included a literature review of previous research that covered different aspects of this work, Chapter 3 included the construction of a biomechanical model, Chapter 4 included the inverse dynamic analysis of the CMJ, Chapter 5 included the use of static optimization to obtain muscle forces, and chapter 6 included the finite element analysis of the human tibia under loads of CMJ.

In Chapter 3, experimental data collection of countermovement jumping of a subject was explained. This included the used of motion capture and force plates to obtain position and ground reaction forces of the subject during trials of countermovement jumping to a maximum height. This experimental data was then analyzed in MATLAB, and an inverse kinematics approach was utilized to obtain joint angles of the hip, knee, and ankle. The ground reaction forces were also analyzed to examine the different stages of a countermovement jump. During jumping, maximum flexion/extension angles of the hip knee and ankle were approximately -105°, 84°, and -35°, respectively. The maximum GRF during jumping was approximately 2.5 BW. During landing, maximum flexion/extension angles of the hip knee and ankle were approximately -44°, 59°, and -35°, respectively. The maximum GRF during jumping was approximately 2.5 BW. All this data was utilized to create a multibody model in MapleSim.

In Chapter 4, inverse dynamics was applied to the multibody model of the subject in MapleSim. Inputs to the model included hip, knee, and ankle joint angles, along with the position data of the pelvis. The main output of this model was the torques about the hip, knee, and ankle. Overall, the torques were larger during landing than during jumping, as expected, given that GRFs are larger during landing. In addition, knee and ankle joint contact forces were computed from the model.

In Chapter 5, static optimization was utilized to solve the problem of redundancy in muscle forces. An analytical and a numerical approach were followed to generate a static optimization to estimate the forces of major muscles in the lower extremity. The objective function of this optimization was to minimize muscle stress, with a power of 3 that correspond to maximum energy expenditure. The optimization problem provided muscle forces for the entire CMJ motion, where muscles with larger moment arms are recruited first. This chapter also included comparisons of using different powers for the objective function and using a different objective function for the motion of countermovement jumping.

In Chapter 6, a human tibia model was utilized in ABAQUS to run a finite element analysis under loads of countermovement jumping. The tibia was modeled as an inhomogeneous isotropic cortical bone. The boundary condition was pinning the distal end of the tibia to only allow axial rotation. The model was loaded with knee and ankle joint contact forces, along with muscle forces of several major muscles with points of insertion/origin on the tibia. Finite element analysis was conducted at three instances of CMJ, which are standing, peak jumping, and peak landing. Stress, strain, and deformation results of the human tibia were obtained and examined. Overall, maximum principal strain was approximately +2056 μstrains during propulsion and approximately +2017 μstrains during landing. A higher localized strain was observed along the anterior crust of the tibial shaft, likely due to lower cross-sectional area and large loads applied during jumping/landing.

With elevated stresses/strains along the tibial shaft during countermovement jumping, risk of injury to the tibia is possible with repetitive jumping that correspond to repetitive impact loads on the bone. The bone is capable of remodeling and adapting to these high impact loads, however, the frequency and magnitude of these forces should be studied further to understand and prevent injury of bones. This work provides a scheme and a step forward into a larger understanding of human motion and how injury takes place with a larger biomechanical insight.

7.2 Limitations

The results of this work show great potential in the field of investigating injury mechanisms and impact loading. However, there are some limitations in the work presented in this thesis.

This work incorporated experimental data of one healthy subject. This caused a limitation in providing substantial observations regarding the motion and its correlation to risk of injury. Due to restrictions in obtaining experimental data, the work was limited to incorporating only one subject. Adding more subjects to the analysis can increase the confidence in the methodology and the results obtained. It can also provide emphasis on the use of subject-specific multibody models and finite element models. To add to that, having more subjects in the study can allow providing further analysis, such as providing insight to specific kinematics or dynamics that lead to higher stress/strain in the bone.

Another limitation was that multibody model constructed in this thesis is a simple 2D model of the subject. This simplification took place as majority of the motion of interest took place in the sagittal plane. This limited the analysis as all muscle forces and joint torques obtained were due to the flexion/extension motions of CMJ, while excluding the effects of abduction/adduction motions and internal/external rotations. To increase the fidelity, multiple enhancements can take place. First, a 3D model of the subject can be constructed. Second, joints (hip, knee, and ankle) were modeled as simple revolute joints. These joints can be modeled as spheres and higher accuracy of joint contact forces can be achieved. In addition, better parameters can be obtained and used for better subject-specific models. This can include the possibility of using imaging techniques (DEXA, CT, or MRI scans) for higher accuracy of parameters such as length, mass, and inertia.

While using a 2D model for the biomechanical multibody model, a 3D model was used for the finite element model of the tibia. Muscle forces were obtained from joint moments of the flexion/extension motion of CMJ. When added as loads in the finite element analysis, the total muscle force was distributed to a 3D component force along the line of action of each muscle. This shift from a 2D multibody model to a 3D finite element model imposed a limitation to the analysis conducted and can be tackled upon incorporating a 3D multibody model.

Validation of joint contact forces from the multibody model and muscle forces from the static optimization were limited in this work. In literature, limited sources document the joint contact forces during jumping, landing, or both. The joint contact forces were closely comparable to previous research and thus were validated to some extent. However, a future work that can be tackled is the possibility of obtaining accurate experimental joint contact forces, during CMJ or vertical jumps, to validate joint contact forces in computational models. Moreover, measuring a muscle force in-vivo is invasive, while measuring muscle activation does not quantify muscle forces. Thus, future work that can be tackled is the possibility of obtaining accurate experimental muscle forces to validate muscle forces obtained. Overall, enhancements are needed in the field of biomechanics to better validate computational models, specifically considering joint contact forces and muscle forces.

Another source of limitation exists from the use of static optimization to obtain muscle forces. In this method, several parameters (maximum isometric forces and physiological cross-sectional areas) of muscles are obtained from literature and thus are not subject-specific. This does not take into account how different individuals have different recruitments of muscles due to different capabilities. For example, an athlete is more likely to have muscles with higher maximum isometric forces than an individual with minimal physical activity. Thus, the problem of static optimization requires parameters and inputs that are more representative of the subject's potential, however, this was limited to available resources and difficulty in measuring these parameters.

Lastly, a limitation to this work was that the tibia model utilized was obtained from a subject that is different from the subject of experimental data collection. Both participants were of similar age, height, and weight. However, for a better analysis of CMJ, it is of interest to have the same subject for both the experimental data collection and the finite element model. This can provide a more meaningful analysis of the motion studied and associated risk of injury.

7.3 Future Work

With the results presented in this work, the methodology could be improved in the future to better analyze the biomechanics of various motions, specifically jumping and landing motions.

1) Experimental data can be collected from athletes of different sports. For example, jumping and landing motions are common in many sports (basketball, volleyball, etc.). These jumps are greatly variable and are completed with different intents, not necessarily reaching a maximum height. The framework in this thesis provides the potential of studying several sports and different types of jumps in each sport. With greater number of subjects and different jumps being analyzed, results of inverse kinematics can provide insight regarding the motion and variability in performance.
2) EMG signals can be collected from subjects during the motion of interest. This can be used to compare muscle activations to muscle forces during the motion. In addition, it can potentially allow investigating the reverse of this framework (forward dynamics).
3) A possible future work can incorporate the reverse of the framework of this thesis, which is through the use of forward dynamics or a hybrid approach of using both inverse and forward dynamics. This method can utilize torques and muscle activation to obtain the optimal countermovement jumps. A reverse of this framework can provide an analysis of different factors that affect the jump and can compare the effects of each loading on the tibial stress and strain. In addition, it can be used as a tool to prevent injury in bone.
4) This work followed a sequential framework of combining multibody dynamic modeling and finite element modeling. A possible future work can enhance this framework into an integrated simultaneous modeling technique for multibody dynamics and finite element analysis. It could provide a better biomechanical analysis of the tibia, directly including dynamic and structural response. This can be possibly achieved by incorporating a flexible tibia with finite element analysis into the multibody model. Currently, computational time and resources (software) do not allow for simultaneous real-time studies and thus development in the field is still required.

8 References

[1] V. Zatsiorsky, *Biomechanics in Sports*, Chichester: John Wiley & Sons, 2008.

[2] M. Bulat, N. Korkmaz Can, Y. Arslan and W. Herzog, "Musculoskeletal Simulation Tools for Understanding Mechanisms of Lower-Limb Sports Injuries", *Current Sports Medicine Reports*, vol. 18, no. 6, pp. 210-216, 2019. Available: 10.1249/jsr.0000000000000601.

[3] M. Fredericson, F. Jennings, C. Beaulieu and G. Matheson, "Stress Fractures in Athletes", *Topics in Magnetic Resonance Imaging*, vol. 17, no. 5, pp. 309-325, 2006. Available: 10.1097/rmr.0b013e3180421c8c.

[4] C. Xu, A. Silder, J. Zhang, J. Hughes, G. Unnikrishnan, J. Reifman, and V. Rakesh, "An Integrated Musculoskeletal-Finite-Element Model to Evaluate Effects of Load Carriage on the Tibia During Walking", *Journal of Biomechanical Engineering*, vol. 138, no. 10, 2016. Available: 10.1115/1.4034216.

[5] A. Alptekin, S. Aritan and E. Harbili, "Investigation of joint reaction forces and moments during the countermovement and squat jump", *Pamukkale Journal of Sport Sciences*, vol. 8, no. 3, pp. 58-71, 2017.

[6] M. McHugh, M. Hickok, J. Cohen, A. Virgile and D. Connolly, "Is there a biomechanically efficient vertical ground reaction force profile for countermovement jumps?", *Translational Sports Medicine*, vol. 4, no. 1, pp. 138-146, 2020. Available: 10.1002/tsm2.200.

[7] D. Cleather, J. Goodwin and A. Bull, "Hip and knee joint loading during vertical jumping and push jerking", *Clinical Biomechanics*, vol. 28, no. 1, pp. 98-103, 2013. Available: 10.1016/j.clinbiomech.2012.10.006.

[8] D. Caruntu and R. Moreno, "Human Knee Inverse Dynamics Model of Vertical Jump Exercise", *Journal of Computational and Nonlinear Dynamics*, vol. 14, no. 10, 2019. Available: 10.1115/1.4044246.

[9] J. Kar and P. Quesada, "A Musculoskeletal Modeling Approach for Estimating Anterior Cruciate Ligament Strains and Knee Anterior–Posterior Shear Forces in Stop-Jumps Performed by Young Recreational Female Athletes", *Annals of Biomedical Engineering*, vol. 41, no. 2, pp. 338-348, 2012. Available: 10.1007/s10439-012-0644-y

[10] S. Davoudabadi Farahani, M. Andersen, M. de Zee and J. Rasmussen, "Optimization-based dynamic prediction of kinematic and kinetic patterns for a human vertical jump from a squatting position", *Multibody System Dynamics*, vol. 36, no. 1, pp. 37-65, 2015. Available: 10.1007/s11044-015-9468-5.

[11] D. Cleather and A. Bull, "Lower-extremity musculoskeletal geometry affects the calculation of patellofemoral forces in vertical jumping and weightlifting", *Journal of Engineering in Medicine*, vol. 224, no. 9, pp. 1073-1083, 2010. Available: 10.1243/09544119jeim731.

[12] A. Hadid, Y. Epstein, N. SHABSHIN and A. Gefen, "Biomechanical Model for Stress Fracture–related Factors in Athletes and Soldiers", *Medicine & Science in Sports & Exercise*, vol. 50, no. 9, pp. 1827-1836, 2018. Available: 10.1249/mss.0000000000001628.

[13] C. Sole, S. Mizuguchi, K. Sato, G. Moir and M. Stone, "Phase Characteristics of the Countermovement Jump Force-Time Curve: A Comparison of Athletes by Jumping Ability", *Journal of Strength and Conditioning Research*, vol. 32, no. 4, pp. 1155-1165, 2018. Available: 10.1519/jsc.0000000000001945.

[14] P. Rice, C. Goodman, C. Capps, N. Triplett, T. Erickson and J. McBride, "Force– and power–time curve comparison during jumping between strength-matched male and female basketball players", *European Journal of Sport Science*, vol. 17, no. 3, pp. 286-293, 2016. Available: 10.1080/17461391.2016.1236840.

[15] P. Cormie, J. McBride and G. McCaulley, "Power-Time, Force-Time, and Velocity-Time Curve Analysis of the Countermovement Jump: Impact of Training", *Journal of Strength and Conditioning Research*, vol. 23, no. 1, pp. 177-186, 2009. Available: 10.1519/jsc.0b013e3181889324.

[16] P. Cormie, M. Mcguigan and R. Newton, "Adaptations in Athletic Performance after Ballistic Power versus Strength Training", *Medicine & Science in Sports & Exercise*, vol. 42, no. 8, pp. 1582-1598, 2010. Available: 10.1249/mss.0b013e3181d2013a.

[17] P. Cormie, M. Mcguigan and R. Newton, "Changes in the Eccentric Phase Contribute to Improved Stretch-Shorten Cycle Performance after Training", *Medicine & Science in Sports & Exercise*, vol. 42, no. 9, pp. 1731-1744, 2010. Available: 10.1249/mss.0b013e3181d392e8.

[18] L. Petrigna, B. Karsten, G. Marcolin, A. Paoli, G., D'antona, A. Palma, and A. Bianco, "A Review of Countermovement and Squat Jump Testing Methods in the Context of Public Health Examination in Adolescence: Reliability and Feasibility of Current Testing Procedures", *Frontiers in Physiology*, vol. 10, 2019. Available: 10.3389/fphys.2019.01384.

[19] A. Sánchez-Sixto, A. Harrison and P. Floría, "Larger Countermovement Increases the Jump Height of Countermovement Jump", *Sports*, vol. 6, no. 4, p. 131, 2018. Available: 10.3390/sports6040131.

[20] A. Salles, V. Baltzopoulos and J. Rittweger, "Differential effects of countermovement magnitude and volitional effort on vertical jumping", *European Journal of Applied Physiology*, vol. 111, no. 3, pp. 441-448, 2010. Available: 10.1007/s00421-010-1665-6.

[21] S. Chavda T. Bromley, P. Jarvis, S. Williams, C. Bishop, A. N. Turner, J. P. Lake, and P. D. Mundy, "Force-Time Characteristics of the Countermovement Jump", *Strength and Conditioning Journal*, vol. 40, no. 2, pp. 67-77, 2018. Available: 10.1519/ssc.0000000000000353.

[22] G. Laffaye, P. Wagner and T. Tombleson, "Countermovement Jump Height", *Journal of Strength and Conditioning Research*, vol. 28, no. 4, pp. 1096-1105, 2014. Available: 10.1519/jsc.0b013e3182a1db03.

[23] D. Robertson, G. Caldwell, J. Hamill, G. Kamen and S. Whittlesey, *Research methods in biomechanics*, Champaign (IL): Human Kinetics, 2014.

[24] M. Ezati, "*Predictive Simulation of Child Gait Using Direct Collocation Optimal Control*", UWspace, 2021.

[25] E. Otten, "Inverse and forward dynamics: models of multi–body systems", *Philosophical Transactions of the Royal Society of London. Series B: Biological Sciences*, vol. 358, no. 1437, pp. 1493-1500, 2003. Available: 10.1098/rstb.2003.1354.

[26] M. King and M. Yeadon, "Advances in the development of whole body computer simulation modelling of sports technique", *Movement & Sport Sciences - Science & Motricité*, no. 90, pp. 55-67, 2013. Available: 10.1051/sm/2013048.

[27] A. Zadpoor and A. Nikooyan, "The relationship between lower-extremity stress fractures and the ground reaction force: A systematic review", *Clinical Biomechanics*, vol. 26, no. 1, pp. 23-28, 2011. Available: 10.1016/j.clinbiomech.2010.08.005.

[28] G. Matheson, D. Clement, D. Mckenzie, J. Taunton, D. Lloyd-Smith and J. Macintyre, "Stress fractures in athletes", *The American Journal of Sports Medicine*, vol. 15, no. 1, pp. 46-58, 1987. Available: 10.1177/036354658701500107.

[29] Z. Altai, E. Montefiori, B. Van Veen, M. A. Paggiosi, E. V. Mccloskey, M. Viceconti, C. Mazza, and X. Li, "Femoral neck strain prediction during level walking using a combined musculoskeletal and finite element model approach", *PLOS ONE*, vol. 16, no. 2, p. e0245121, 2021. Available: 10.1371/journal.pone.0245121.

[30] F. Mo, J. Li, M. Dan, T. Liu and M. Behr, "Implementation of controlling strategy in a biomechanical lower limb model with active muscles for coupling multibody dynamics and finite element analysis", *Journal of Biomechanics*, vol. 91, pp. 51-60, 2019. Available: 10.1016/j.jbiomech.2019.05.001.

[31] L. Shu, K. Yamamoto, J. Yao, P. Saraswat, Y. Liu, M. Mitsuishi, and N. Sugita, "A subject-specific finite element musculoskeletal framework for mechanics analysis of a total knee replacement", *Journal of Biomechanics*, vol. 77, pp. 146-154, 2018. Available: 10.1016/j.jbiomech.2018.07.008.

[32] E. Grood and W. Suntay, "A Joint Coordinate System for the Clinical Description of Three-Dimensional Motions: Application to the Knee", *Journal of Biomechanical Engineering*, vol. 105, no. 2, pp. 136-144, 1983. Available: 10.1115/1.3138397.

[33] G. Wu, S. Siegler, P. Allard, C. Kirtley, A. Leardini, D. Rosenbaum, M. Whittle, D. D. D'Lima, L. Cristofolini, H. Witte, O. Schmid, and I. Stokes, "ISB recommendation on definitions of joint coordinate system of various joints for the reporting of human joint motion—part I: ankle, hip, and spine", *Journal of Biomechanics*, vol. 35, no. 4, pp. 543-548, 2002. Available: 10.1016/s0021-9290(01)00222-6.

[34] R. Bisseling and A. Hof, "Handling of impact forces in inverse dynamics", *Journal of Biomechanics*, vol. 39, no. 13, pp. 2438-2444, 2006. Available: 10.1016/j.jbiomech.2005.07.021.

[35] D. Winter, *Biomechanics and motor control of human movement*. Hoboken, N.J.: Wiley, 2009.

[36] K. Moran and E. Wallace, "Eccentric loading and range of knee joint motion effects on performance enhancement in vertical jumping", *Human Movement Science*, vol. 26, no. 6, pp. 824-840, 2007. Available: 10.1016/j.humov.2007.05.001.

[37] M. Pandy, "Computer Modeling and Simulation of Human Movement", *Annual Review of Biomedical Engineering*, vol. 3, no. 1, pp. 245-273, 2001. Available: 10.1146/annurev.bioeng.3.1.245.

[38] R. Crowninshield and R. Brand, "A physiologically based criterion of muscle force prediction in locomotion", *Journal of Biomechanics*, vol. 14, no. 11, pp. 793-801, 1981. Available: 10.1016/0021-9290(81)90035-x.

[39] M. Klein Horsman, H. Koopman, F. van der Helm, L. Prosé and H. Veeger, "Morphological muscle and joint parameters for musculoskeletal modelling of the lower extremity", *Clinical Biomechanics*, vol. 22, no. 2, pp. 239-247, 2007. Available: 10.1016/j.clinbiomech.2006.10.003.

[40] G. Yamaguchi, *Dynamic modeling of musculoskeletal motion*. Springer, 2001.

[41] D. Cleather, J. Goodwin and A. Bull, "An Optimization Approach to Inverse Dynamics Provides Insight as to the Function of the Biarticular Muscles During Vertical Jumping", *Annals of Biomedical Engineering*, vol. 39, no. 1, pp. 147-160, 2010. Available: 10.1007/s10439-010-0161-9.

[42] B. Prilutsky and V. Zatsiorsky, "Optimization-Based Models of Muscle Coordination", *Exercise and Sport Sciences Reviews*, vol. 30, no. 1, pp. 32-38, 2002. Available: 10.1097/00003677-200201000-00007.

[43] D. Tsirakos, V. Baltzopoulos and R. Bartlett, "Inverse Optimization: Functional and Physiological Considerations Related to the Force-Sharing Problem", *Critical Reviews in Biomedical Engineering*, vol. 25, no. 4-5, pp. 371-407, 1997. Available: 10.1615/critrevbiomedeng.v25.i4-5.20.

[44] B. van Bolhuis and C. Gielen, "A comparison of models explaining muscle activation patterns for isometric contractions", *Biological Cybernetics*, vol. 81, no. 3, pp. 249-261, 1999. Available: 10.1007/s004220050560.

[45] F. Michaud, M. Lamas, U. Lugrís and J. Cuadrado, "A fair and EMG-validated comparison of recruitment criteria, musculotendon models and muscle coordination strategies, for the inverse-dynamics based optimization of muscle forces during gait", *Journal of NeuroEngineering and Rehabilitation*, vol. 18, no. 1, 2021. Available: 10.1186/s12984-021-00806-6.

[46] S. Delp, *Surgery simulation: A computer graphics system to analyze and design musculoskeletal reconstructions of the lower limb*, Stanford Univ, 1990.

[47] M. Carhart and G. Yamaguchi, *Biomechanical analysis of compensatory stepping: implications for paraplegics standing via functional neuromuscular stimulation*, Arizona State University, 2021.

[48] C. Au and J. Dunne, "*Gait 2392 opensim model*", 2013.

[49] D. Cleather and A. Bull, "An Optimization-Based Simultaneous Approach to the Determination of Muscular, Ligamentous, and Joint Contact Forces Provides Insight into Musculoligamentous Interaction", *Annals of Biomedical Engineering*, vol. 39, no. 7, pp. 1925-1934, 2011. Available: 10.1007/s10439-011-0303-8.

[50] M. Sharif Shourijeh, "Optimal Control and Multibody Dynamic Modelling of Human Musculoskeletal Systems", *UWspace*, 2013. Available: http://hdl.handle.net/10012/7570.

[51] I. Haider, M. Baggaley and W. Brent Edwards, "Subject-Specific Finite Element Models of the Tibia With Realistic Boundary Conditions Predict Bending Deformations Consistent With In Vivo Measurement", *Journal of Biomechanical Engineering*, vol. 142, no. 2, 2019. Available: 10.1115/1.4044034.

[52] J. Rho, "An ultrasonic method for measuring the elastic properties of human tibial cortical and cancellous bone", *Ultrasonics*, vol. 34, no. 8, pp. 777-783, 1996. Available: 10.1016/s0041-624x(96)00078-9.

[53] A. Speirs, M. Heller, G. Duda and W. Taylor, "Physiologically based boundary conditions in finite element modelling", *Journal of Biomechanics*, vol. 40, no. 10, pp. 2318-2323, 2007. Available: 10.1016/j.jbiomech.2006.10.038.

[54] D. Zhao, S. Banks, D. D'Lima, C. Colwell and B. Fregly, "In vivo medial and lateral tibial loads during dynamic and high flexion activities", *Journal of Orthopaedic Research*, vol. 25, no. 5, pp. 593-602, 2007. Available: 10.1002/jor.20362.

[55] N. H. Hart, S. Nimphius, T. Rantalainen, A. Ireland, A. Siafarikas, and R. U. Newton, "Mechanical basis of bone strength: influence of bone material, bone structure and muscle action", J Musculoskelet Interact, vol.17, no. 3, 114-139, 2017/

[56] S. Bhavikatti, *Finite element analysis*. New Delhi: New Age International (P) Ltd., 2005.

[57] E. Morgan, G. Unnikrisnan and A. Hussein, "Bone Mechanical Properties in Healthy and Diseased States", *Annual Review of Biomedical Engineering*, vol. 20, no. 1, pp. 119-143, 2018. Available: 10.1146/annurev-bioeng-062117-121139.

[58] R. Al Nazer, J. Lanovaz, C. Kawalilak, J. Johnston and S. Kontulainen, "Direct in vivo strain measurements in human bone—A systematic literature review", *Journal of Biomechanics*, vol. 45, no. 1, pp. 27-40, 2012. Available: 10.1016/j.jbiomech.2011.08.004.

[59] C. Ruiz Wills, A. L. Olivares, S. Tassani, M. Ceresa, V. Zimmer, M. A. Gonzalez Ballester, L. M. Del Rio, L. Humbert, and J. Noailly, "3D patient-specific finite element models of the proximal femur based on DXA towards the classification of fracture and non-fracture cases", *Bone*, vol. 121, pp. 89-99, 2019. Available: 10.1016/j.bone.2019.01.001.